University of São Paulo
"Luiz de Queiroz" College of Agriculture

Development of sprinkler with adjustable orifice using iris-type mechanism for variable rate irrigation

Luiz Ricardo Sobenko

Thesis presented to obtain the degree of Doctor in Science.
Area: Agricultural Systems Engineering

Piracicaba
2019

Luiz Ricardo Sobenko
Agronomist

Development of sprinkler with adjustable orifice using iris-type mechanism for variable rate irrigation

versão revisada de acordo com a resolução CoPGr 6018 de 2011

Advisor:
Prof. Dr. TARLEI ARRIEL BOTREL

Thesis presented to obtain the degree of Doctor in Science.
Area: Agricultural Systems Engineering

Piracicaba
2019

Dados Internacionais de Catalogação na Publicação
DIVISÃO DE BIBLIOTECA – DIBD/ESALQ/USP

Sobenko, Luiz Ricardo

Development of sprinkler with adjustable orifice using de iris-type mechanism for variable rate irrigation / Luiz Ricardo Sobenko. - - versão revisada de acordo com a resolução CoPGr 6018 de 2011. - - Piracicaba, 2019.

52 p.

Tese (Doutorado) - - USP / Escola Superior de Agricultura “Luiz de Queiroz”.

1. Impressão 3D 2. Irrigação de precisão 3. Manufatura aditiva 4. Padrões de distribuição de água I. Título

I dedicate with love to
my parents Luiz Carlos and Vera Lúcia
my sister Luciane
my brother in law Jeferson
my niece Nicole
and my friends.

ACKNOWLEDGEMENTS

God.

All my family. Thanks especially to my parents, Luiz Carlos and Vera Lúcia, my sister Luciane, my brother in law Jeferson and my niece Nicole for their continuous love, help and support.

The "Luiz de Queiroz" College of Agriculture – University of São Paulo (ESALQ/USP) and the Graduate Program in Agricultural Systems Engineering (PPGESA) for the opportunity and education during my doctoral study.

The Coordination for the Improvement of Higher Education Personnel (CAPES) for providing the scholarship in this research.

My advisor Dr. Tarlei Arriel Botrel for having trusted in my potential to be his last graduate student, for his friendship, patience, knowledge provided, and especially for his humility, which were essential during my master and doctoral periods.

The Professors (and friends) Dr. Antonio Pires de Camargo (FEAGRI/UNICAMP), Dr. José Antonio Frizzone (ESALQ/USP) and Dr. Sergio Nascimento Duarte (ESALQ/USP) patience, support, knowledge provided, scientific discussions and talks.

The researchers Dr. Marcelo Fernandes de Oliveira and Dr. Jorge Vicente Lopes da Silva from Renato Archer Information Technology Centre (CTI) for all their technical and material supports in this research.

My lab colleagues Diego Sousa, Rogério Lavanholi and Wagner Bombardelli for all their support, talks and friendship.

My colleagues from Biosystems Engineering Department (LEB), especially Bruno Lena, Eder Fanaya Jr., Ezequiel Saretta, Fabrício Correia, Geancarlo Takanori, Jéfferson Costa, Jefferson Vieira, Jéssica Garcia, João Paulo, Marcus Talamini, Otávio Neto, Timóteo Herculino and Wagner Wolff.

Professors from LEB, especially Fábio Ricardo Marin, Jarbas Honório de Miranda, Marcos Vinícius Folegatti and Rubens Duarte Coelho.

Employees from LEB Ângela Silva, Antônio Agostinho, Áureo Santana, Beatriz Novaes, Davilmar Colevatti, Francisco de Oliveira, Gilmar Batista Grigolon, Luís Custódio, Luiz Fernando and Paula Bonassa.

All my friends from Piracicaba, especially Allan Patrick, Amanda Avelar, Bruna Bacco, Jéssica Drum, Maicon Javorski, Pamela Dutra, Perla Oliveira, and Ricardo Feliciano.

Lastly, everyone who supported me in any way throughout my doctoral period.

Don't point out faults, point solutions.

Henry Ford

CONTENTS

RESUMO

Desenvolvimento de aspersor com orifício ajustável utilizando mecanismo tipo íris para uso em irrigação em taxa variada

A irrigação em taxa variada tem a intenção de fornecer água, identificando "quando", "onde" e "quanto" deve-se aplicar, resultando em uso otimizado da água, aumento da produtividade agrícola, economia de energia e diminuição da lixiviação de nutrientes. Primeiramente, o conceito de um aspersor de orifício ajustável usando um mecanismo tipo íris, acionado por um motor de passo, para uso em irrigação em taxa variada foi proposto e desenvolvido. Um protótipo foi fabricado usando técnicas de manufatura aditiva. Suas características operacionais foram avaliadas. Para predizer a vazão, um modelo determinístico que representa a operação do aspersor foi proposto e validado. Em um segundo momento, para verificar a adequação dos padrões de distribuição de água do protótipo, aspersores convencionais com placas defletoras rotativas e fixas (RSPSs e FSPSs, respectivamente) foram acoplados a este, cada um equipado com duas placas defletores diferentes, sendo que testes em laboratório foram realizados. Sobreposições matemáticas também foram realizadas para simular espaçamentos entre aspersores de 2 e 3 m. Os principais resultados mostraram que: (1) os coeficientes de descarga observados variaram de acordo com as condições de operação, sendo 0,530 quando o orifício foi totalmente aberto e um valor médio de 0,636 quando o mecanismo íris reduziu a seção do orifício; (2) para a condição de um orifício parcialmente aberto, ocorreu o fenômeno de inversão de jato, fazendo com que o jato se tornasse assimétrico; (3) as uniformidades de aplicação simuladas de linha lateral em operação foram 61,2-91,6% e 88,5-98,7% para FSPSs e RSPSs, respectivamente sob diferentes condições de espaçamento entre aspersores; (4) FSPSs apresentaram elevado potencial de escoamento superficial.

Palavras-chave: Impressão 3D, Irrigação de precisão, Manufatura aditiva, Padrões de distribuição de água

ABSTRACT

Development of sprinkler with adjustable orifice using iris-type mechanism for variable rate irrigation

Variable rate irrigation intends to supply water identifying "when", "where" and "how much" should be apply, resulting in optimised use of water, increased crop productivity, energy saving and decreased nutrient leaching. Firstly, the concept of an adjustable orifice sprinkler using an iris mechanism actuated by a stepper motor for use in variable rate irrigation was proposed and developed. A prototype was manufactured using additive manufacturing techniques. Its operational characteristics were evaluated. To predict the flow rate, a deterministic model that represented the operation of the sprinkler was proposed and validated. Secondly, to verify the suitability of the water distribution patterns of prototype, rotating and fixed spray plate sprinklers (RSPSs and FSPSs, respectively) were attached to this, each equipped with two different deflector plates, to the mechanism. Tests indoors were performed. Mathematical overlaps were also performed for 2 and 3 m sprinkler spacing. The main results showed that: (1) The observed discharge coefficients varied according to the operating conditions, these being 0.530 when the orifice was fully opened and an average of 0.636 when the iris mechanism reduced the orifice section; (2) for the condition of a partially opened orifice, the phenomenon of jet inversion occurred causing the jet to become asymmetrical; (3) the simulated sprinkling uniformities of lateral line travel were 61.2–91.6% and 88.5–98.7% for FSPSs and RSPSs respectively under different sprinkler spacing conditions; (4) FSPSs presented high potential for surface runoff.

Keywords: 3D printing, Additive manufacturing, Precision irrigation, Water distribution patterns

ABBREVIATION LIST

CFD	Computational fluid dynamics
CTI	Renato Archer Information Technology Centre
EEPROM	Electrically erasable programmable ready-only memory
ESALQ	College of Agriculture "Luiz de Queiroz"
FDM	Fused deposition modelling
FSPS	Fixed spray plate sprinkler
ISO	International Organization for Standardization
LEMI	Irrigation testing laboratory
PA	Precision agriculture
PWM	Pulse-width modulation
RMSE	Root mean square error
RSPS	Rotating spray plate sprinkler
STL	Standard triangle language
USB	Universal serial bus
USP	University of São Paulo
VRI	Variable rate irrigation

SYMBOL LIST

B / B'	Blade edge in the initial and movement conditions (m)
C_c	Contraction coefficient (dimensionless)
C_d	Discharge coefficient (dimensionless)
C_v	Velocity coefficient (dimensionless)
CUC	Christiansen coefficient of uniformity (%)
D	Orifice diameter (m)
g	Gravitational acceleration (m s^{-2})
h	Precipitation rate (mm h^{-1})
h_i	Precipitation rate of the *i*-th observation (mm h^{-1})
$\bar{h}$	Average precipitation rate (mm h^{-1})
H	Operation pressure head (m)
n	Number of observations
q	Flow rate (m^3 s^{-1})
r / r'	Orifice radius in the initial and movement conditions (m)
r_1, r_2 / r_1', r_2'	Segments of orifice radius in the initial and movement conditions (m)
R	Correlation coefficient (dimensionless)
R^2	Determination coefficient (dimensionless)
S / S'	Section flow in the initial and movement conditions (m^2)
S_C	Opening section of the collector (m^2)
t	Test duration (h)
V	Volume collected in each collector (dm^3)
X_1, X_2, X_3 / X_1', X_2', X_3'	Sides of the triangle in the initial and movement conditions (m)
Z_1, Z_2 / Z_1', Z_2'	Segments of X_2 in the initial and movement conditions (m)
$\alpha_1, \alpha_2, \alpha_3$ / $\alpha_1', \alpha_2', \alpha_3'$	Internal angles of the triangle in the initial and movement conditions (degrees)
β	Micro-stepper motor angle (degrees)

I. GENERAL INTRODUCTION

In agriculture, most of the water use is intended for the irrigation technique. Increasingly, its management has been evolving into a priority issue, with the aim of better management to optimize agricultural production and water resources uses.

In terms of irrigation techniques, the systems are still designed and managed considering that the area is homogeneous, neglecting the spatial variability of the physical and hydraulic soil parameters, which results in a relatively constant irrigation depth throughout the area (Sobenko et al., 2018). If the applied depth is insufficient to the crop, water stress will occur and, consequently, yield reduction is expected to occur. Excessive depths will lead to leaching of nutrients and eventual soil erosion, impairment of soil physical and chemical characteristics, and contribute to the waste of water and nutrients as well (Al-Kufaishi et al., 2006; Pan et al., 2013).

In this context, since the 1990s, variable rate irrigation (VRI) emerges as a possible solution, since it addresses the spatiotemporal heterogeneity in the field (topography, soil type, water storage capacity and cropping systems), with a view to identifying "when", "where" and "how much" water to apply, resulting in optimised use of water and other environmental resources; increased crop productivity; energy saving; and decreased nutrient leaching (Kranz et al., 2012; Haghverdi et al., 2016).

Centre pivots and linear-move sprinkler machines are commonly used as pressurised irrigation systems all over the world and present high potential irrigation efficiency (Faci et al., 2001; Frizzone et al., 2018). These sprinkler irrigation systems are suitable for variable rate application development due to their wide coverage area, high level of automation and are increasingly used by farmers (Kranz et al., 2012; Evans et al., 2013). In these systems, the variable rate application can be done by adjusting the travelling speed of the equipment displacement (sector control) or adjusting the irrigation depth in each individual sector by changing the sprinkler discharge (zone control). With regard to the commercially available technology for zone control, the mechanism for controlling the sprinkler discharge is based on the duty cycle of a solenoid valve installed at the inlet of each emitter, i.e. pulse-width modulation (PWM). However, due to the numerous cycles of opening/closing solenoid valves, pressure regulators may have their lifespan reduced. Furthermore, there are concerns about how the on/off cycles influence water distribution patterns and application uniformity (King and Kincaid, 2004; Dukes and Perry, 2006).

Herein, it is proposed a novel concept of an adjustable orifice sprinkler for irrigation using the iris-type mechanism to vary its section. Iris-type mechanisms are usually formed by a

combination of overlapped metal blades that form an adjustable orifice enabling control of orifice sizes. Therefore, we believe in a potential of using this mechanism, actuated by a micro-stepper motor, to adjust the orifice section of sprinklers used in centre pivot or linear-move for VRI systems. It can present advantages in relation to the PWM technique, such as: the possibility of obtaining sections of nozzle closer to the theoretical, and, consequently, greater flexibility and accuracy to apply the desired depth; less wear of the device in relation to the continuous operation of the solenoid valves; and lower losses in the uniformity of water distribution at the moment when there is variation of pressure at the emitter input.

The objectives of this research, separated into two chapters, were (1) to develop an adjustable orifice sprinkler using an iris mechanism; to evaluate its operational characteristics; to propose a deterministic model to predict the flow rate of sprinklers with the adopted mechanism; and, (2) to verify its water distribution patterns coupled to different deflector plates and under discharge adjustments to demonstrate its suitability for VRI.

REFERENCES

Al-Kufaishi, S. A., Blackmore, B. S., and Sourell, H. (2006). The feasibility of using variable rate water application under a central pivot irrigation system. **Irrigation and Drainage Systems**, 20, 317–327.

Dukes, M. D., and Perry, C. (2006). Uniformity testing of variable-rate center pivot irrigation control systems. **Precision Agriculture**, 7, 205–212.

Evans, R. G., Larue, J., Stone, K. C., and King, B. A. (2013). Adoption of site-specific variable rate sprinkler irrigation systems. **Irrigation Science**, 31, 871–887.

Faci, J. M., Salvador, R., Playán, E., and Sourell, H. (2001). Comparison of fixed and rotating spray plate sprinklers. **Journal of Irrigation and Drainage Engineering**, 127(4), 224–233.

Frizzone, J. A., Rezende, R., Camargo, A. P., and Colombo, A. (2018). **Irrigação por aspersão: sistema pivô central**. Maringá: Eduem.

Haghverdi, A., Leib, B. G., Washington-Allen, R. A., Buschermohle, M. J., and Ayers, P. D. (2016). Studying uniform and variable rate center pivot irrigation strategies with the aid of site-specific water production functions. **Computers and Electronics in Agriculture**, 123, 327–340.

King, B. A., and Kincaid, D. C. (2004). A variable flow rate sprinkler for site-specific irrigation management. **Applied Engineering in Agriculture**, 20(6), 765–770.

Kranz, W. L., Evans, R. G., Lamm, F. R., O'Shaughnessy, S. A., and Peters, R. T. (2012). A review of mechanical move sprinkler irrigation control and automation technologies. **Applied Engineering in Agriculture**, 28(3), 389–397.

Pan, L., Adamchuk, V. I., Martin, D. L., Schroeder, M. A., and Ferguson, R. B. (2013). Analysis of soil water availability by integrating spatial and temporal sensor-based data. **Precision Agriculture**, 14, 414–433.

Sobenko, L. R., Armindo, R. A., Wolff, W., Costa, J. O., Miranda, J. H., and Duarte, S. N. (2018). Estimation of second season maize yield loss by the spatial variability of the soil physical-water properties. **Bioscience Journal**, 34(3), 1257–1265.

2. AN IRIS MECHANISM FOR VARIABLE RATE SPRINKLER IRRIGATION

Abstract

Variable rate irrigation intends to supply water at the right time and place in order to improve water-use efficiency, save energy and decrease nutrient leaching. The concept of an adjustable orifice sprinkler using an iris mechanism actuated by a stepper motor for use in variable rate irrigation was proposed and developed. A prototype was manufactured using additive manufacturing techniques. Its operational characteristics were evaluated. To predict the flow rate, a deterministic model that represented the operation of the sprinkler was proposed and validated. The observed discharge coefficients varied according to the operating conditions, these being: 0.530 when the orifice was fully opened; and an average of 0.636 when the iris mechanism reduced the orifice section. For the condition of a partially opened orifice, the phenomenon of jet inversion occurred causing the jet to become asymmetrical. The proposed concept allows flowrates closer to the required values to be obtained and consequently provides greater flexibility and accuracy to applying the target irrigation depth.

Keywords: 3D printing, Additive manufacturing, Adjustable orifice, Development, Precision irrigation, Site-specific irrigation

2.1. Introduction

As water supplies become limited due to competition from encroaching urbanisation, efforts to maximise irrigation efficiency will have to increase to irrigate the same land area with fewer resources (Dukes and Perry, 2006). Globally, about 70% of freshwater is used for agriculture, with irrigation the major user of water (Hedley and Yule, 2009). Thus, irrigation management has evolved into a high priority issue (Haghverdi et al., 2016).

Precision agriculture has been seeking approaches to improve agricultural processes by considering the variability of spatialetemporal production factors (Armindo et al., 2010). Variable rate irrigation (VRI) intends to supply water to crops in a precise quantity, at the right time and place in order to improve water-use efficiency, thereby increasing productivity, saving energy and decreasing nutrient leaching (Pan et al., 2013).

Centre pivots and linear-move sprinkler machines are commonly used as pressurised irrigation systems all over the world and present high potential irrigation efficiency (Faci et al., 2001). These sprinkler irrigation systems are suitable for variable rate application development due to their wide coverage area, high level of automation and are increasingly used by farmers (Kranz et al., 2012; Evans et al., 2013). Moreover, the potential water conservation and the efficiency of centre-pivot and linear-move irrigation systems may be enhanced by applying variable amounts of water along the lateral line to correspond with variable soil or crop conditions (Dukes and Perry, 2006). Hedley and Yule (2009) compared VRI to conventional uniform irrigation methods and found that 9-19% of irrigation water was saved.

Research has justified the use of precision irrigation through modelling to establish scheduling of irrigation by management zones (Haghverdi et al., 2015; Ceresoli et al., 2016; Miller et al., 2018). Commercially available technologies for VRI enable sector and zone control. Sector control technologies are simpler and allow a limited number of rectangular sectors for linear-move systems or several pieslice shaped sectors for centre pivots. In this case, the variable rate application occurs due to changes in the travelling speed, but the discharge of the emitters remains unchanged. On the other hand, zone control technologies are more complex and enable to adjust the irrigation depth in each individual sector by changing the output of emitters. The mechanism for controlling the flow rate of each sprinkler is based on the duty cycle of a solenoid valve installed at the inlet of each emitter, i.e. pulse-width modulation (PWM). However, due to the numerous cycles of opening/closing solenoid valves, pressure regulators may have their lifespan reduced. Furthermore, there are concerns about how the on/off cycles influence water distribution patterns and application uniformity (King and Kincaid, 2004; Dukes and Perry, 2006). For anhydrous ammonia application, Bora et al. (2005) evaluated the reliability of a variable-rate system using PWM solenoids cycling at 15 Hz for 60 h. The authors could not estimate the lifespan of the valves, but 84% of them operated effectively in these conditions. Han et al. (2001) evaluated a variable-rate control system consisted of PWM solenoids in several individual nozzles for nitrogen application. By the volumetric tests carried out, the results showed that the primary causes of the inaccuracy are the valve-to-valve differences in flow rate response to PWM signals, presenting calibration erros ranging from – 15 to 20%.

On the development of zone control technologies, King and Kincaid (2004) and Armindo et al. (2010) proposed prototypes of sprinklers for centre pivots or linear-move systems. The discharge of their prototypes was adjusted by displacing an internal concentric rod that changes the nozzle flow section. King and Kincaid (2004) reported that the spray became finer and the wetted radius decreased about 15% due to the interference of the rod in the flow through the nozzle. Both researches indicated that variable rate sprinklers based on a concentric pin that moves into a sprinkler nozzle bore was a feasible concept.

Another potential approach for obtaining variable discharge emitters consists of using an iris or diaphragm mechanism to adjust the flow cross-section of an orifice. Iris-type mechanisms are usually formed by a combination of overlapped metal blades that form an adjustable orifice enabling control of aperture sizes and have been used in several applications such as imaging systems (Ren et al., 2012), optics (Syms et al., 2004), radiotherapy (Graves et al., 2007), energy beam collimators (Hill, 1984), lens technology (Chang et al., 2000), robotic radiosurgery (Echner et al., 2009), and solar reactors (Rajan et al., 2016).

Here, an adjustable orifice sprinkler using an iris mechanism was developed for use in VRI. We believe this to be a novel concept. The operational characteristics of the developed sprinkler were measured and a deterministic model was proposed to predict the flow rate of sprinklers with the adopted mechanism.

2.2. Material and methods

The sprinkler prototype was developed and evaluated at the Irrigation Testing Laboratory (LEMI) of the College of Agriculture "Luiz de Queiroz" (ESALQ/USP), Piracicaba, São Paulo State, Brazil.

2.2.1. Prototype design and manufacturing

The prototype was designed using Solid Edge ST7 (Siemens Product Lifecycle Software Inc., Plano, TX, USA) software (Figure 2.1). The basic components of the proposed emitter are: (1) blade holder; (2) micro-stepper motor; (3) motion or driving gear; (4) blades; (5) central body; (6) driven gear; (7) frame/support for coupling deflector plate; (8) micro-stepper motor housing; and, (9) threaded screw for mounting the components of the sprinklers (Figure 2.1).

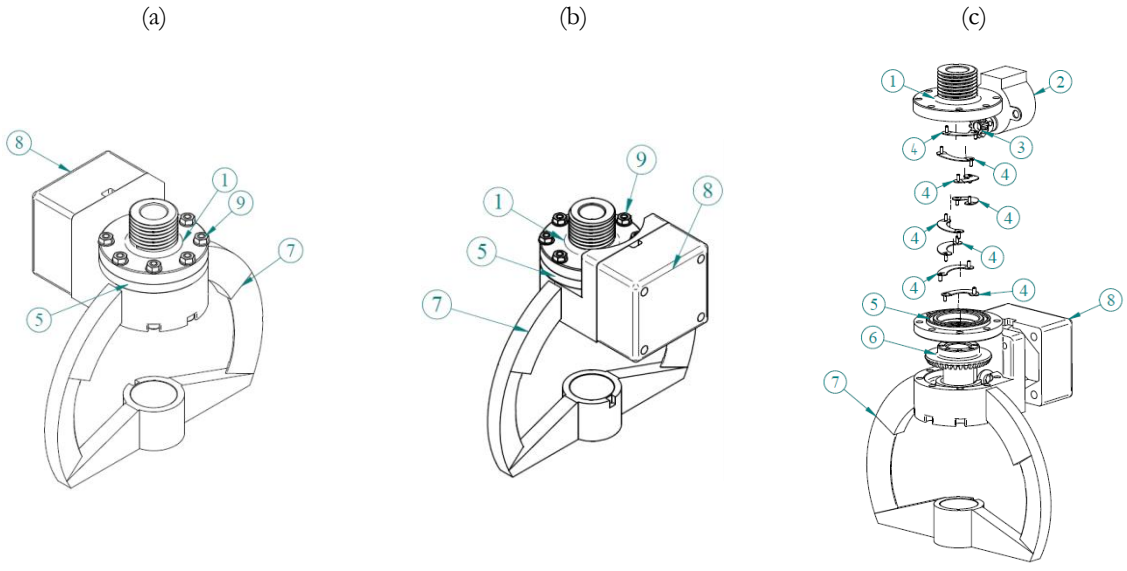

Figure 2.1. Basic components of the developed prototype: perspective views (a and b); and, assembly view (c).

The iris mechanism was designed with eight blades (Figure 2.2a) to provide flow sections of approximately circular shape, however the orifice is adjusted for higher or lower discharges. Each blade has two guide pins, one centralised and the other towards the end,

represented by elements (4.1) and (4.2) of Figure 2.2a, respectively. These pins are responsible for the movement of the blades, in addition to assisting the overlap between them. Also, the blades are 0.5 mm thick and were designed to enable adjusting the orifice diameter from 4.9 to 12 mm, corresponding to a range of values compatible with commercial nozzles (Fabrimar, 2018; Senninger, 2018). Lower aperture sizes are mechanically possible but would require higher torque from the stepper motor.

The designed blade holder (Figure 2.2b) has threads to enable coupling of the sprinkler to its hydraulic fittings (1.1); a cavity for housing the sealing rings, which are responsible for sealing the top of the blade assembly (1.2); screw holes (1.3); and smaller cavities (1.4) serving as housing for the blade pins (4.1).

The central body (Figure 2.2c) has the following functions: to limit the movement of the blades; to join the blades, the blade holder and the driven gear; and, sealing. The central body has two cavities for sealing rings.

Two gears were designed to enable adjusting the position of the overlapped blades and consequently the orifice aperture size. The transmission ratio between them was 1:3, i.e. every three laps of the motion/driving gear (Figure 2.2d) causes one full turn of the driven gear (Figure 2.2e). The motion/driving gear has 12 straight teeth (Figure 2.2f), while the driven gear has 36 straight teeth (Figure 2.2e).

Finally, by Figures 2.2g, 2.2h and 2.2i, the union of the elements (1), (2), (3), (4), (5) and (6) compose the prototype sprinkler. In addition, in order to enable the use of the prototype in practical applications, a structure was designed for the coupling deflector plates and the micro-stepper motor (Figures 2.2j and 2.2k). A case to protect the micro-stepper motor against water droplets was also designed (Figure 2.2l).

After designing, the components solid models were produced in Standard Triangle Language (STL) format, the prototype was then manufactured using additive manufacturing techniques, also known as "3D printing", at the Three-Dimensional Technologies Laboratory, Renato Archer Information Technology Centre (CTI), Campinas, São Paulo State, Brazil.

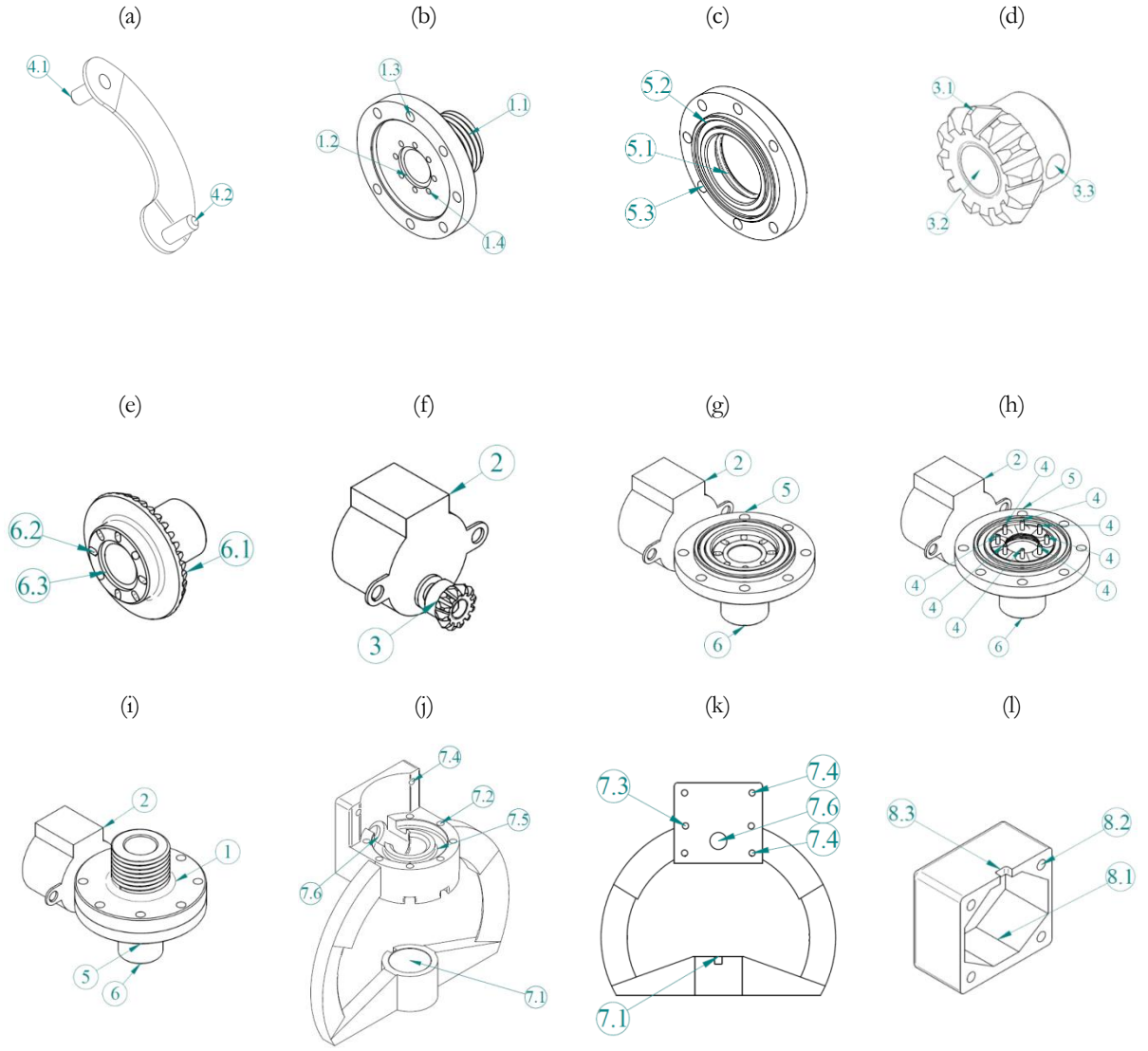

Figure 2.2. Detail of the components of the developed prototype: blade (a), blade holder (b), central body (c), motion/driving gear (d), driven gear (e), coupling between the motor shaft and the drive gear (f), sprinkler assembly (g, h and i), structure (j and k), and micro-stepper motor protection (l).

The Magics RP (Materialise Inc., Leuven, Belgium) software was used by the CTI to read the STL files and interface with the machines, edit and repair some designing errors, as well to prepare the build platform. The techniques employed for manufacturing the prototype were Polyjet, and Fused Deposition Modelling (FDM), both currently a technology of Stratasys Inc. (Valencia, CA, USA). The Polyjet technique was applied for the production of elements (1), (3), (5) and (6), by the use of an acrylic photopolymer jetted via high-resolution inkjet and cured using ultraviolet light, that offers high surface quality (Esses et al., 2011). The acrylic polymer used was the VeroClear-LGD820 resin in a Connex 350 (Stratasys Inc.) equipment, which operated in the "digital material" build mode with layer thickness resolution of 28 μm.

The elements (7) and (8) were produced by the FDM technique, which, despite its simplicity in relation to Polyjet, is characterised by its mechanical, thermal and chemical resistance (Schmitz et al., 2018). In this technique a polymer, such as acrylonitrile-butadiene-styrene (ABS), in the form of filaments, was partially melted and then extruded to perform layer-by-layer deposition (Kollamaram et al., 2018) in a Fortus 400 (Stratasys Inc.) machine with layer thickness resolution of 100 μm. The additive manufacturing techniques utilised provided functional prototypes with high accuracy of complex geometries as designed. Therefore, additive manufacturing appears as a powerful tool for rapid development of concepts and experiments.

The blades of the iris mechanism were made of AISI 304 stainless steel and manufactured using laser cutting. The blades were made of stainless steel in order to: i) ensure resistance to operating pressure; ii) ensure mechanical strength; iii) ensure non-oxidation due to frequent exposure to water and chemicals; and, iv) have adequate flexibility and thickness that allow adequate overlap between the blades due to the torque supplied by the motor.

The housing cavities of the sealing rings as well as the screw holes for screws were designed for standard sizes and manufacturers easily found in the local market.

2.2.2. Electronic system and calibration for adjusting the orifice flow section

Figure 2.3 shows three possible aperture sizes of the orifice controlled by the micro-stepper motor. Several techniques could have been used to enable adjusting the orifice aperture size, but the simplest technique that was sufficient to validate the concept of the sprinkler. An Arduino platform (www.arduino.cc) was employed to provide means for controlling the micro-stepper motor and thus to adjust the orifice aperture size. Arduino is an open source single-board microcontroller based on easy-to-use hardware and software. It is programmed using a Wiring-based language similar to C++. Boards can be purchased as pre-assembled or do-it-yourself kits, and hardware design is available. In this research, the Arduino UNO R3, a microcontroller board based on the ATMega380 chip (Atmel, Datasheet 380), was used. It has 14 digital input/output pins and 6 analogue inputs that provide 10 bits of resolution. The ATMega380 also has a 16 MHz crystal oscillator, a USB (universal serial bus) connection, a power jack and a reset button. It uses a flash memory of 32 KB with 0.5 KB used for boot loading, 2 KB of SRAM and 1 KB of EEPROM (Electrically Erasable Programmable Ready-Only Memory).

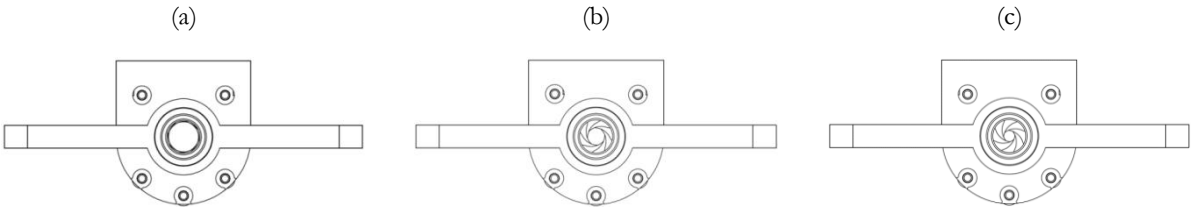

Figure 2.3. Top view of various graduated openings of the developed prototype orifice.

The integrated circuit ULN2003A (Texas Instruments Inc., Dallas, TX, USA) was employed as interface circuit required to drive the stepper motor (Figure 2.4). ULN2003A is an integrated circuit of high current (up to 500 mA) Darlington arrays, each containing seven open collector common emitter pairs. The integrated circuit also includes suppression diodes for inductive load driving. The stepper motor moves in response to the sequence in which its internal coils are turned on; hence driving the stepper motor is operated in a simple matter of pulsing digital outputs of the microcontroller.

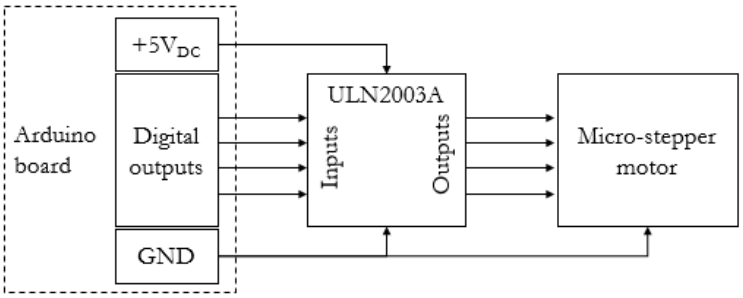

Figure 2.4. Block diagram of the circuit for driving the micro-stepper motor.

The micro-stepper motor used was the model 28BYJ-48 (Kiatronics Inc., Tauranga, New Zealand), whose technical specifications are presented in Table 2.1. This low-cost motor was easily obtained and had sufficient torque to drive the gears.

Table 2.1. Technical specifications of 28BYJ-48 micro-stepper motor.

Tension	Reduction	Shaft diameter	Step angle	Steps per revolution	Frequency	Resistance	Torque
5 V_{DC}	1/64	3 mm	0.088°	4,075.77	100 Hz	50 Ω ±7%	34.3 μN m

2.2.3. Theoretical modelling for flow predicting

Each step (or step-motor angle) was generated by the motor providing a corresponding change in the orifice flow section. In Figure 2.5A the iris mechanism with one of its blades at its initial condition, that is when the orifice section is at a maximum. The radius of the orifice in the initial condition (r) is given by the sum of r_1 and r_2, the latter being subtracted from the blade's edge (B). Thus, by tracing a circumference of radius from the centre of the orifice to the centre of the blade's (4.1) guide pin, an initial triangle of sides X_1, X_2 and X_3 and internal angles α_1, α_2 and α_3 is obtained. As the measurements of the sides of this triangle in the initial condition are known by the design, the cosine law can be applied to determine the internal angles:

$$X_1^2 = X_2^2 + X_3^2 - 2X_2X_3\cos(\alpha_2) \quad (2.1)$$

$$X_2^2 = X_1^2 + X_3^2 - 2X_1X_3\cos(\alpha_3) \quad (2.2)$$

$$X_3^2 = X_1^2 + X_2^2 - 2X_1X_2\cos(\alpha_1) \quad (2.3)$$

where:

X_1, X_2, and X_3 - sides of the triangle in the initial condition (m); and

α_1, α_2, and α_3 - internal angles of the triangle in the initial condition (degrees).

After the micro-stepper motor is actuated, each step corresponds to a rotation of the driven gear, due to the transmission ratio of 3:1, and consequently to the movement of the blade. In this way, the sides X_1 and X_2 of the triangle remain constant, whereas the measure of X_3' will vary with the step of the motor (X_3'), causing variation in the internal angles as well (α_1', α_2' and α_3') (Figure 2.5b).

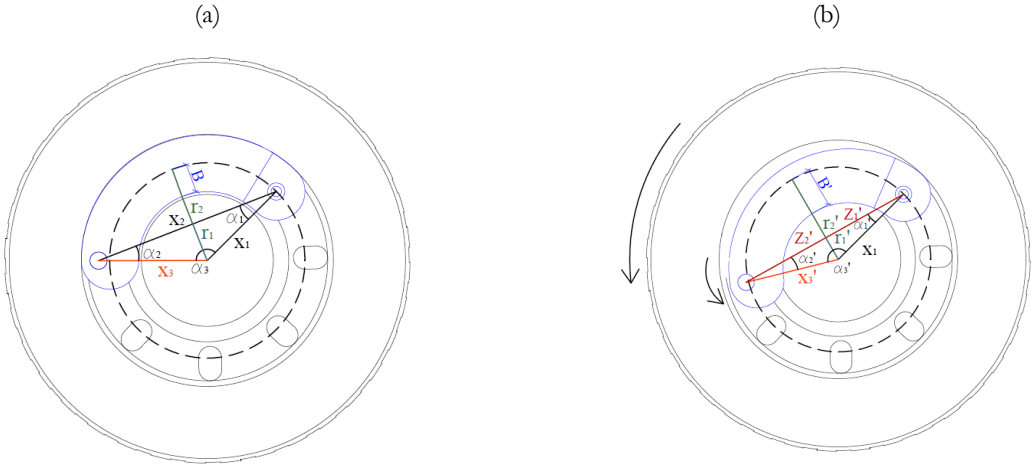

Figure 2.5. Section variation schematic by the stepper motor angle in the initial (A) and blade movement (B) conditions.

Firstly, the radius r_1 in the initial condition is easily calculated by trigonometric relation as a function of X_3 and α_2 (Equation 2.4).

$$r_1 = X_3 \sin(\alpha_2) \tag{2.4}$$

where:

r_1 - segment of orifice radius in the initial condition (m).

To determine r_2 in the same condition, the X_2 side can be divided into two segments (Z_1 and Z_2), these being also calculated by trigonometric relations (Equations 2.5 and 2.6).

$$Z_1 = X_1 \cos(\alpha_1) \tag{2.5}$$

$$Z_2 = X_3 \cos(\alpha_2) \tag{2.6}$$

where:

Z_1 and Z_2 - segments of X_2 in the initial condition (m).

In this way, r_2 can be calculated by applying the reduced equation of the circumference, i.e. for the circumference with the centre at the origin (Equation 2.7). The calculation of the "x" and "y" coordinates of the equation is represented in Equation (2.8). Rearranging the terms, r_2 in the initial condition can be calculated by Equation (2.9).

$$x^2 + y^2 = r^2 \tag{7}$$

$$[r \cos(\alpha_1) - Z_2]^2 + (r_1 + r_2)^2 = r^2 \tag{8}$$

$$r_2 = \sqrt{r^2 - [r \cos(\alpha_1) - Z_2]^2} - r_1 \tag{9}$$

where:

x and y - coordinates of the reduced equation of the circumference (m);

r - orifice radius in the initial condition (m); and

r_2 - segment of orifice radius in the initial condition (m).

Secondly, with the stepper motor drive, the α_3' angle will vary with the sum of each motor step angle ($\alpha_3 + i_{angle}$). From Equation (2.2), the X_3' side could be calculated by iteration for each step angle of the motor. This also allowed the calculation of the new α_1' and α_2' internal angles by Equations (2.3) and (2.1), respectively.

With the variation of X_3, consequently, Z_1, Z_2, r_1, r_2 and B will also vary (Figure 2.5b). Therefore, the variation of the radius of the orifice (r') is represented by the sum of the variation of its radius segments (r_1' and r_2'), subtracted from the variation of the blade's edge (B'). Equation (2.10) describes the variation of the section (S') of the developed prototype orifice as a function of the motor step angle.

$$S' = \pi r'^2$$

$$S' = \pi(r_1' + r_2' - B')^2 \tag{10}$$

$$S' = \pi\left\{[X_3' \sin(\alpha_2')] + \left[\sqrt{r^2 - (r\cos(\alpha_1) - Z_2')^2} - r_1\right] - B'\right\}^2$$

where:

S' - section flow in the movement condition (m^2);

r' - orifice radius in the movement condition (m);

r_1' and r_2' - segments of orifice radius in the moviment condition (m);

B' - blade edge in the movement condition (m);

X_3' - side of the triangle in the movement condition (m); and

Z_2' - segment of X_2 in the movement condition (m).

As described, for each motor step angle, there is an increase or reduction of the section of the orifice, providing flow variation. For the estimation of the orifice flow, Equation (2.11) is commonly used, and, when replacing Equation (2.10) in Equation (2.11), a theoretical model is developed that allows the flow through the orifice to be predicted when using the variable rate iris mechanism (Equation 2.12).

$$q = C_d\, S \sqrt{2gH} \tag{11}$$

$$q = C_d\, \pi\left\{[X_3' \sin(\alpha_2')] + \left[\sqrt{r^2 - (r\cos(\alpha_1) - Z_2')^2} - r_1\right] - B'\right\}^2 \sqrt{2gH} \tag{12}$$

where:

q - flow rate ($m^3\ s^{-1}$);

C_d - discharge coefficient (dimensionless);

α_2' - internal angle of the triangle in the movement condition (degrees);

g - gravitational acceleration ($m\ s^{-2}$); and

H - operation pressure head (m).

2.2.4. Sprinkler operational characterisation

In sprinkler nozzle studies, the determination of the flow versus pressure head, as well as their discharge coefficients, represents their most important operational characteristics. Tests were carried out to determine flow versus pressure curves under seven orifice opening diameters: 10.86, 10.04, 9.32, 8.34, 6.94, 6.31 and 4.93 mm. Dimensional measurements of the orifice flow section were made by a HB400 (Starrett Inc., Athol, MA, USA) horizontal benchtop optical comparator. For each opening section, tests were carried out at operation pressures of 70 to 250 kPa, in increments of 30 kPa.

Tests were undertaken in a testing bench equipped with a pump, variable frequency driver, pressure and temperature transmitters installed at the inlet of the prototype and electromagnetic flow meter (Figure 2.6).

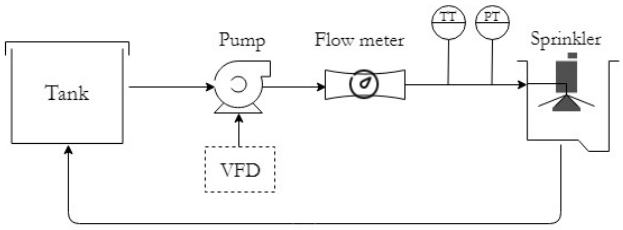

Figure 2.6. Instrumentation diagram of the testing bench used for operational tests of the developed prototype: variable frequency driver (VFD), temperature transmitter (TT) and pressure transmitter (PT).

Discharge coefficients were determined as a function of the testing pressure and orifice section, isolating the "C_d" term from Equation (2.11).

With the flow values observed in the tests, for each operation pressure, the theoretical model was assessed using the root mean square error (RMSE) and graphical error analysis. The RMSE is a common index to measure the accuracy of models that quantify differences between observed and estimated values (Duran-Ros et al., 2010; Provenzano et al., 2015). The graphical error analysis is also useful to quantify prediction errors while evaluating the accuracy of models because it provides prediction errors associated with their frequency of occurrence (Vilaça et al., 2017).

2.3. Results and discussion

Figure 2.7a shows all components of the prototype developed, and Figure 2.7b shows the assembled prototype.

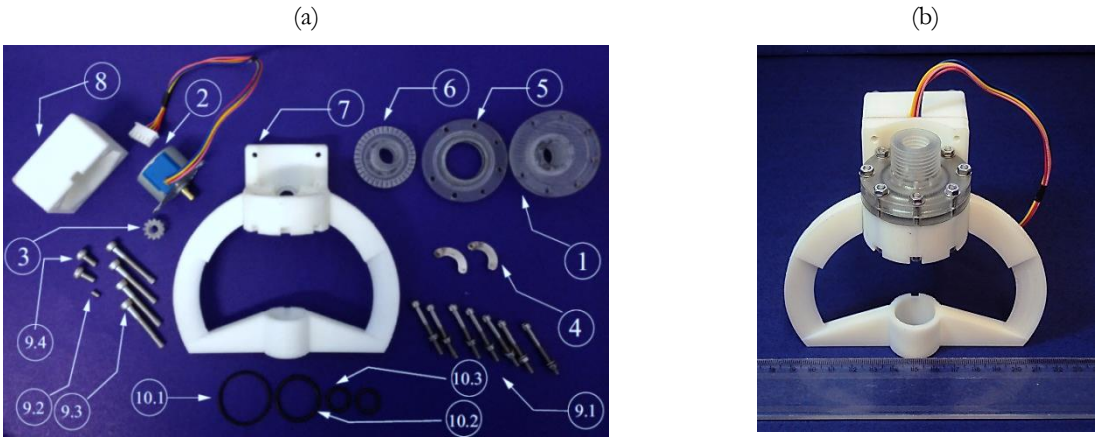

Figure 2.7. Images of the prototype.

The relationship between flow and pressure is one of the hydraulic characteristics that directly influences the performance of an irrigation system (Frizzone et al., 2012). Figure 2.8 presents curves of flow rate as a function of pressure under seven area sections within the range the prototype was designed to operate. The characteristic equations of the prototype, for each orifice diameter tested and motor step angle, as well as their determination coefficients (R^2) are shown in Table 2.2. By the R^2 values, there is proper goodness of fitting between observed data and power-law equations.

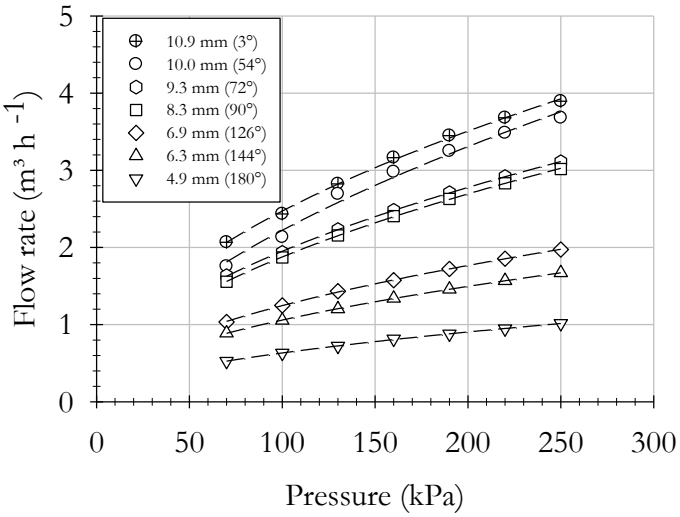

Figure 2.8. Characteristic curves of flow versus pressure, for different orifice diameters and motor step angles of the developed prototype.

Table 2.2. Characteristic equation, determination coefficient (R^2) and discharge coefficient (C_d) for various orifice diameters (D) and motor step angles.

D (mm)	Motor step angle (degrees)	Equation	R^2	C_d
10.86	3°	$q = 0.242H^{0.505}$	0.998	0.530
10.04	54°	$q = 0.159H^{0.573}$	0.988	0.572
9.32	72°	$q = 0.170H^{0.521}$	0.999	0.570
8.34	90°	$q = 0.186H^{0.510}$	0.999	0.688
6.94	126°	$q = 0.123H^{0.503}$	0.999	0.655
6.31	144°	$q = 0.107H^{0.498}$	0.999	0.671
4.93	180°	$q = 0.059H^{0.515}$	0.999	0.662

The obtained discharge coefficients (C_d) are also shown in Table 2.2. According to Azevedo Netto and Fernandez y Fernandez (2015), C_d is the product of the velocity (C_v) and contraction (C_c) coefficients, and it depends on the shape and conditions of the orifice. The lowest C_d value was observed for the condition when the orifice is fully opened, i.e. the iris mechanism's blades did not influence the flow. In this operating condition, due to the design of the prototype, the orifice behaves as a short cylindrical outer tube, i.e. a cylindrical tube which projects out of the wall of the device.

For situations where the iris mechanism begins to reduce the orifice cross-section, a common thin-walled orifice, or an orifice plate, is characterised, and an average C_d = 0.636 was observed. The values are close to the mean value of 0.605 observed by Hobbs and Humphreys (1990), the value of 0.609 simulated in computational fluid dynamics (CFD) by Reader-Harris and Hodges (2012), and the 0.61 suggested by Azevedo Netto and Fernandez y Fernandez (2015) for practical applications.

For conventional sprinkler nozzles used in centre-pivot systems, discharge coefficient values are often higher. Silva et al. (2015) when testing commercial sprinklers of three different brands obtained values ranging from 0.88 to 0.98. This is due to the fact that the nozzles were of convergent conical type and more efficient in terms of energy loss. Azevedo Netto and Fernandez y Fernandez (2015) commented that the high C_d values for this type of nozzle are due to a combination of the angle of divergence and the length of the tube, which should be about nine times the diameter of the contraction section.

The type of blade designed for the iris mechanism of the developed prototype approximates a conventional sprinkler orifice for use in irrigation. However, as the blades overlap it has been observed that a perfect circle is not formed and irregular geometry occurs. At this point the phenomenon of jet inversion occurred, and the jet ceased to be axisymmetric and become an asymmetric (Thomas et al., 1991). This phenomenon often occurs when jets pass

through different cross sections in successive stages, changing their original shape, from that in the contraction section.

In the literature, only examples of this phenomenon are presented for simple orifice geometries such as circular, elliptic, triangular and square (Azevedo Netto and Fernandez y Fernandez, 2015; Li et al., 2017). Thomas et al. (1991), when studying the effect of orifice geometry on the shape of jets, found that jets from circular orifices spread more rapidly along their minor axis, making them circularly symmetrical after a short distance. On the other hand, the authors point out that, through hydrodynamic theory, that jets emerging from irregular orifices may eventually become axisymmetric as eddies on the periphery of the jet obliterate the detailed geometry of the proximal core. However, the distance required for the jet circularisation to become symmetrical is unknown.

Figure 2.9a shows the fitting scattering data, correlation coefficient (R) and RMSE values as well of the predicted flow rate by the model. Using the measured C_d values based on motor step angle (Table 2.2), the flow rate values predicted by the model presented a strong correlation with the observed values, as well a low RMSE value, which indicates the accuracy of the model.

Also, in the proposed model, relative errors lower than 10% were observed in 72.5% of the predictions, while 95% of predictions presented relative errors of up to 34% (Figure 2.9b). These errors are due to uncontrolled factors such as gaps between the junctions of the constituent elements.

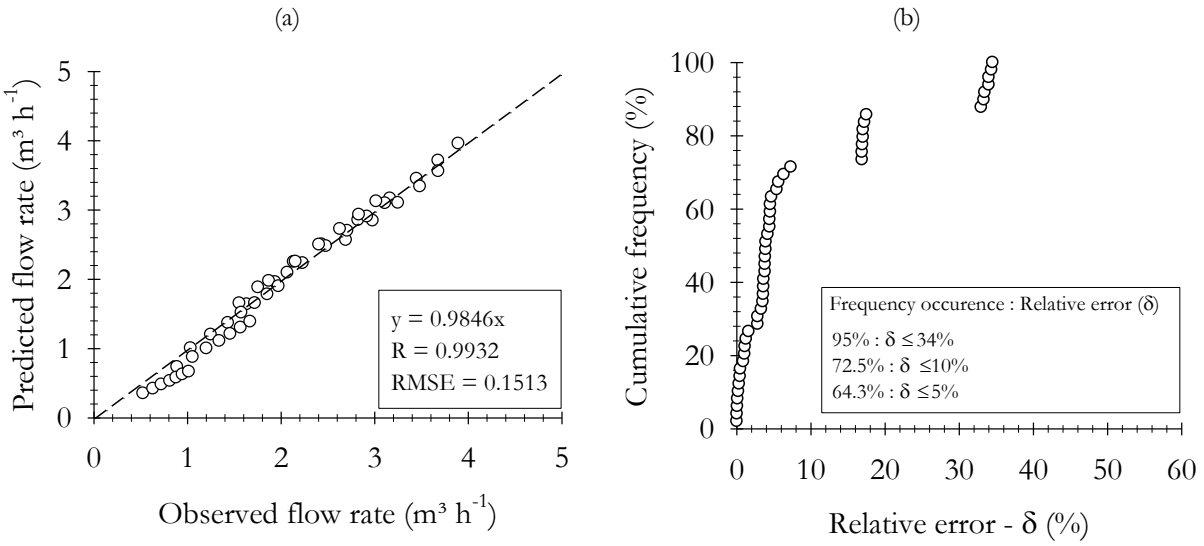

Figure 2.9. Accuracy indicators of the model developed to estimate the flow rate from the prototype.

Thus, future studies with regard to the phenomenon of jet dispersion provided by the iris mechanism are suggested, aiming at solutions for this, such as design improvements or the development of specific deflector plates which adapt to the type of asymmetric circularisation due to the geometrical characteristics of the formed orifice, as well as assist in an improvement in distribution uniformity patterns.

2.4. Conclusions

A novel concept for a variable rate irrigation sprinkler was proposed. Laboratory evaluations were carried out to determine basic operational characteristics of the prototype. The iris or diaphragm mechanism controlled by a stepper motor enabled accurate flow control over the range of flow sections varying from 4.9 to 12 mm in diameter, which produced flow rates close to the theoretical model, and consequently provided greater flexibility and accuracy when applying the target irrigation depth.

A deterministic model was developed and validated to predict the flow rate of sprinklers with the iris mechanism.

References

Armindo, R. A., Botrel, T. A., and Garzella, T. G. (2010). Flow rate sprinkler development for site-specific irrigation. **Irrigation Science**, 29, 233–240.

Azevedo Netto, J. M., and Fernandez y Fernandez, M. (2015). **Manual de hidráulica (9th ed.)**. São Paulo: Blucher.

Bora, G. C., Schrock, M. D., Oard, D. L., Grimm, J. J., Kolb, T. C., and Higgins, J. J. (2005). Reliability tests of pulse width modulation (PWM) valves for flow rate control of anhydrous ammonia. **Applied Engineering in Agriculture**, 21(6), 955–960.

Ceresoli, L. L., Sobenko, L. R., Kreitlov, B., and Armindo, R. A. (2016). Variabilidade espacial dos atributos físico-hidráulicos do solo em uma área e estimativa da lâmina de irrigação de precisão. **Irriga**, Edição Especial, 179–190.

Chang, G., Peng, J., and Chan, C. (2000). **Multi-blade lens-aperture control mechanism**, U.S. Patent No. 6,161,966.

Dukes, M. D., and Perry, C. (2006). Uniformity testing of variable-rate center pivot irrigation control systems. **Precision Agriculture**, 7, 205–212.

Duran-Ros, M., Arbat, G., Barragán, J., Ramírez de Cartagena, F., and Puig-Bargués, J. (2010). Assessment of head loss equations developed with dimensional analysis for micro irrigation filters using effluents. **Biosystems Engineering**, 106, 521–526.

Echner, G. G., Kilby, W., Lee., M, Earnst, E., Sayeh, S., Schlaefer, A., Rhein, B., Dooley, J. R., Lang, C., Blanck, O., Lessard, E., Maurer Jr, C. R., and Schlegel, W. (2009). The design, physical properties and clinical utility of an iris collimator for robotic radiosurgery. **Physics in Medicine and Biology**, 54, 5359–5380.

Esses, J. S., Berman, P., Bloom, A. I., and Sosna, J. (2011). Clinical application of physical 3D models derived from MDCT data and created by rapid prototyping. **American Journal of Roentgenology**, 196, 683–688.

Evans, R. G., Larue, J., Stone, K. C., and King, B. A. (2013). Adoption of site-specific variable rate sprinkler irrigation systems. **Irrigation Science**, 31, 871–887.

Fabrimar. (2018). **Performance table**. Retrieved from http://www.fabrimar.com.br/categoria?irrigacao=produtos-para-pivo-central..

Faci, J. M., Salvador, R., Playán, E., and Sourell, H. (2001). Comparison of fixed and rotating spray plate sprinklers. **Journal of Irrigation and Drainage Engineering**, 127(4), 224–233.

Frizzone, J. A., De Freitas, P. S. L., Rezende, R., and De Faria, M. A. (2012). **Microirrigação: Gotejamento e microaspersão**. Maringá: Eduem.

Graves, E. E., Zhou, H., Chatterjee, R., Keall, P. J., Gambhir, S. S., Contag, C. H., and Boyer, A. L. (2007). Design and evaluation of a variable aperture collimator for conformal radiotherapy of small animals using a microCT scanner. **Medical Physics**, 34(11), 4359–4367.

Haghverdi, A., Leib, B. G., Washington-Allen, R. A., Ayers, P. D., and Buschermohle, M. J. (2015). Perspectives on delineating management zones for variable rate irrigation. **Computers and Electronics in Agriculture**, 117, 154–137.

Haghverdi, A., Leib, B. G., Washington-Allen, R. A., Buschermohle, M. J., and Ayers, P. D. (2016). Studying uniform and variable rate center pivot irrigation strategies with the aid of site-specific water production functions. **Computers and Electronics in Agriculture**, 123, 327–340.

Han, S., Hendrickson, L. L., Ni, B., and Zhang, Q. (2001). Modification and testing of a commercial sprayer with PWM solenoids for precision spraying. **Applied Engineering in Agriculture**, 17(5), 591–594.

Hedley, C. B., and Yule, I. J. (2009). Soil water status mapping and two variable-rate irrigation scenarios. **Precision Agriculture**, 10(4), 342–355.

Hill, R. (1984). **Variable aperture collimator for high energy radiation**, U.S. Patent No. 4,450,578.

Hobbs, J. M., and Humphreys, J. S. (1990). The effect of orifice plate geometry upon discharge coefficient. **Flow Measurement and Instrumentation**, 1, 133–140.

King, B. A., and Kincaid, D. C. (2004). A variable flow rate sprinkler for site-specific irrigation management. **Applied Engineering in Agriculture**, 20(6), 765–770.

Kollamaram, G., Croker, D. M., Walker, G. M., Goyanes, A., Basit, A. W., and Gaisford, S. (2018). Low temperature fused deposition modeling (FDM) 3D printing of thermolabile drugs. **International Journal of Pharmaceutics**, 545, 144–152.

Kranz, W. L., Evans, R. G., Lamm, F. R., O'Shaughnessy, S. A., and Peters, R. T. (2012). A review of mechanical move sprinkler irrigation control and automation technologies. **Applied Engineering in Agriculture**, 28(3), 389–397.

Li, X., Zhou, R., Yao, W., and Fan, X. (2017). Flow characteristic of highly underexpanded jets from various nozzle geometries. **Applied Thermal Engineering**, 125, 240–253.

Miller, K. A., Luck, J. D., Heeren, D. M., Lo, T., Martin, D. L., and Barker, J. B. (2018). A geospatial variable rate irrigation control scenario evaluation methodology based on mining root zone available water capacity. **Precision Agriculture**, 19, 666–683.

Pan, L., Adamchuk, V. I., Martin, D. L., Schroeder, M. A., and Ferguson, R. B. (2013). Analysis of soil water availability by integrating spatial and temporal sensor-based data. **Precision Agriculture**, 14, 414–433.

Provenzano, G., Alagna, V., Autovino, D., Juarez, J. M., and Rallo, G. (2015). Analysis of geometrical relationships and friction losses in small-diameter lay-flat polyethylene pipes. **Journal of Irrigation and Drainage Engineering**, 142(2), 04015041.

Rajan, A., Abouseada, M., Manghaipathy, P., Ozalp, N., Majid, F. A., Salem, A., and Srinivasa, A. (2016). An experimental and analytical study on the feasibility of SMA spring driven actuation of an iris mechanism. **Applied Thermal Engineering**, 105, 849–861.

Reader-Harris, M., and Hodges, N. B. D. (2012). The effect of contaminated orifice plates on the discharge coefficient. **Flow Measurement and Instrumentation**, 25, 2–7.

Ren, L., Park, S., Ren, H., and Yoo, I. (2012). Adaptive liquid lens by changing aperture. **Journal of Microelectromechanical Systems**, 21(4), 953–958.

Schmitz, D. P., Ecco, L. G., Dul, S., Pereira, E. C. L., Soares, B. G., Barra, G. M. O., and Pegoretti, A. (2018). Electromagnetic interference shielding effectiveness of ABS carbon-based composites manufactured via fused deposition modelling. **Materials Today Communications**, 15, 70–80.

Senninger. (2018). **Mechanized irrigation: low pressure – high performance**. Retrieved from: https://www.senninger.com/sites/senninger.hunterindustries.com/files/senninger-pivot-irrigation-products-catalog.pdf.

Silva, R. M., Coelho, R. D., Faria, L. A., and Maschio, R. (2015). Coeficiente de descarga em emissores de pivô central. Engenharia Agrícola, **Journal of the Brazilian Association of Agricultural Engineering (SBEA)**, 35(3), 419–429.

Syms, R. R. A., Zou, H., Stagg, J., and Veladi, H. (2004). Sliding-blade MEMS íris and variable optical attenuator. **Journal of Micromechanics and Microengineering**, 14, 1700–1710.

Thomas, J. D., O'Shea, J. P., Rodriguez, L., Popovic, D. A., Svizerro, T., and Weyman, A. E. (1991). Impact of orifice geometry on the shape of jets: an in vitro Doppler color flow study. **Journal of the American College of Cardiology**, 17(4), 901–908.

Vilaça, F. N., Camargo, A. P., Frizzone, J. A., Mateos, L., and Koech, R. (2017). Minor losses in start connectors of microirrigation laterals. **Irrigation Science**, 35, 227–240.

3. PERFORMANCE OF AN IRIS MECHANISM EQUIPPED WITH FIXED AND ROTATING DEFLECTOR PLATES FOR VARIABLE RATE SPRINKLER IRRIGATION

Abstract

Technologies have been developed for variable rate irrigation (VRI) systems to apply water based on the spatial and temporal variability of field conditions. To verify the suitability of the water distribution patterns of an iris-type mechanism applied in VRI systems, rotating and fixed spray plate sprinklers (RSPSs and FSPSs, respectively) were attached to this, each equipped with two different deflector plates, to the mechanism. Tests indoors were performed under the following conditions: iris mechanism orifices 4.93 and 6.94 mm in diameter, a sprinkler at a height of 0.91 m above the ground, an operating pressure of 103 kPa. Mathematical overlaps were also performed for 2- and 3-m sprinkler spacing. The results showed that: (1) individual FSPSs distributed water with higher intensity over a smaller distance from the sprinkler than RSPSs, which distributed water at a lower application rate but over a greater distance; (2) the simulated sprinkling uniformities of lateral line travel were 61.2–82.5% and 88.5–98.6% for FSPSs and RSPSs respectively under different sprinkler spacing conditions; (3) the uniformity of sprinkling decreased by up to 19.7% for FSPSs and 6.7% for RSPSs with increasing overlap in spacing; (4) FSPSs presented high potential for surface runoff; (5) the phenomenon of jet inversion did not affect the uniformity of the iris mechanism's water distribution, especially for RSPSs.

Keywords: 3D printing, Additive manufacturing, Adjustable orifice, Precision irrigation, Site-specific irrigation, Uniformity, Water distribution patterns

3.1. Introduction

Precision agriculture (PA) comprises a set of techniques and methodologies that aim to optimize crop management and the use of agricultural inputs, thus providing maximum economic efficiency and crop production. In this area, technologies focus on the existence of in-field variability, or the site-specific aspects, of natural components, including chemical leaching, runoff, drainage, water content, nutrients and soil components (Dong et al., 2013). Within the field of PA, one aspect is variable rate irrigation (VRI), studied since the 1990s with a view to identifying "when", "where" and "how much" water to apply according to the spatial and temporal variability of field characteristics, such as topography, soil type, water storage capacity and cropping systems, inter alia, and thus develop appropriate technologies (Stone et al., 2006). In this regard, self-propelled centre pivot and linear move sprinkler irrigation systems have been found to be particularly suitable technologies for VRI because of their high level of automation, ease of use and large area coverage with a single irrigation lateral line (Evans et al., 2012; Kranz et al., 2012).

Commercially available technologies for VRI make it possible to control the amount of water applied in each sector and zone. Focusing on centre pivot systems, which currently

comprise about 99% of the self-propelled sprinkler market (Evans et al., 2012), the earliest VRI technique was sector control, which used a simple methodology to alter the water application depth through the mechanical adjustment of the speed of lateral travel; this allowed the division of the irrigated area into several pie-slice shaped sectors. In contrast, zone control technologies enable the adjustment of the irrigation depth in each individual sector by changing the discharge rate of sprinklers.

The commercially available mechanism for controlling the flow rate of each sprinkler is based on the duty cycle of a solenoid valve installed at the inlet of each sprinkler, i.e. pulse-width modulation (PWM). However, there are concerns in terms of how the on/off cycles influence the water distribution patterns and uniformity of application of this technology (King and Kincaid, 2004; Dukes and Perry, 2006). Other methods have been under development to address varying application depths along the moving irrigation lateral line. The variable flow sprinkler developed by King and Kincaid (2004) uses a mechanically activated pin to alter the discharge section area, adjusting the sprinkler flow rate based on operating pressure. However, the main concern with this approach is that the wetted pattern and size distribution of water droplets of the sprinkler change with the flow rate, creating issues for the uniformity of water application with a change in sprinkler pattern overlap.

According to Sourell et al. (2003), the characteristics of spray plate sprinklers, sprinkler spacing and machine speed will define irrigation performance in all self-propelled sprinkler irrigation systems. Frizzone et al. (2018) also point out that to obtain a more uniform water pattern, sprinklers must be spaced in such a way that each point in the ground receives water from at least three sprinklers. A wide range of sprinkler device types are available in centre pivot irrigation systems, from conventional impact sprinklers with different types of nozzles, to various types of low-pressure spray plate sprinklers. Impact sprinklers have been replaced by low-pressure spray plate sprinklers, commonly classified as fixed spray plate sprinklers (FSPSs) and rotating spray plate sprinklers (RSPSs), which produce very different droplet size distributions and water application patterns (Faci et al., 2001; DeBoer, 2002; Sourell et al., 2003; Sayyadi et al., 2014; Jiao et al., 2017). FSPSs are based on the impact of a water jet on a fixed grooved plate, comprising various numbers or sizes of grooves to break up the water jet into discrete water droplets. RSPSs can be equipped with different grooved spray plates that rotate under the effect of the water jet, creating momentum on the plate itself; these sprinklers were developed to provide greater jet lengths and lower application rates (Frizzone et al., 2018). Comparing FSPSs and RSPSs, the first type is cheaper and more robust, while the second type presents a more

uniform water distribution pattern and greater adaptability to field conditions (Ouazaa et al., 2014).

With the objective of advancing a novel sprinkler concept to be applied in the VRI technique, in a previous work, Sobenko et al. (2018) developed a prototype using an iris-type mechanism actuated by a micro-stepper motor to vary the discharge section, presenting its complete construction and operating characteristics. This prototype allowed flow rates closer to those required in the field than other means, as well as greater flexibility and accuracy in applying water to the target irrigation depth. However, it was noted that when the orifice section of the iris mechanism was reduced, the phenomenon of jet inversion occurred, causing the jet to become asymmetrical, which could impair the water distribution patterns. Further investigation of the water distribution patterns was thus required.

Therefore, in this paper an improvement on the prototype previously developed to enable coupling to any commercial sprinkler was reported, i.e. as an accessory for sprinkler discharge control. The main objective was to verify the water distribution patterns of the prototype coupled to fixed and rotating deflector plates and under discharge adjustments to demonstrate its suitability for variable rate sprinkler irrigation.

3.2. Material and methods

The VRI sprinkler prototype was evaluated in indoor conditions (without wind) at the Irrigation Testing Laboratory (LEMI) of the College of Agriculture "Luiz de Queiroz" (ESALQ/USP), Piracicaba, São Paulo State, Brazil. Its development and operational characteristics are described in full in Sobenko et al. (2018).

3.2.1. Improvements to the prototype

The "structure" component of the VRI sprinkler prototype was modified by replacing the side flaps with a commercial thread ½" (Item 7.1 in Figure 3.1b). With this modification, the prototype can be used as an "accessory" device that can be coupled to commercially available sprinklers to apply water at variable rates (Figure 3.1).

The new element (Item 7.1 in Figure 3.1) was manufactured using Polyjet's additive manufacturing technique at the Three-Dimensional Technologies Laboratory, Renato Archer Information Technology Centre (CTI), Campinas, São Paulo State, Brazil. The Polyjet technique was applied using an acrylic photopolymer jetted via high-resolution inkjet and cured using

ultraviolet light, which offers a high surface quality (Esses et al., 2011). The acrylic polymer used was the VeroClear-LGD820 resin in a Connex 350 (Stratasys Inc., Valencia, CA, USA) 3D printer, operated in the "digital material" build mode with a layer thickness resolution of 28 μm.

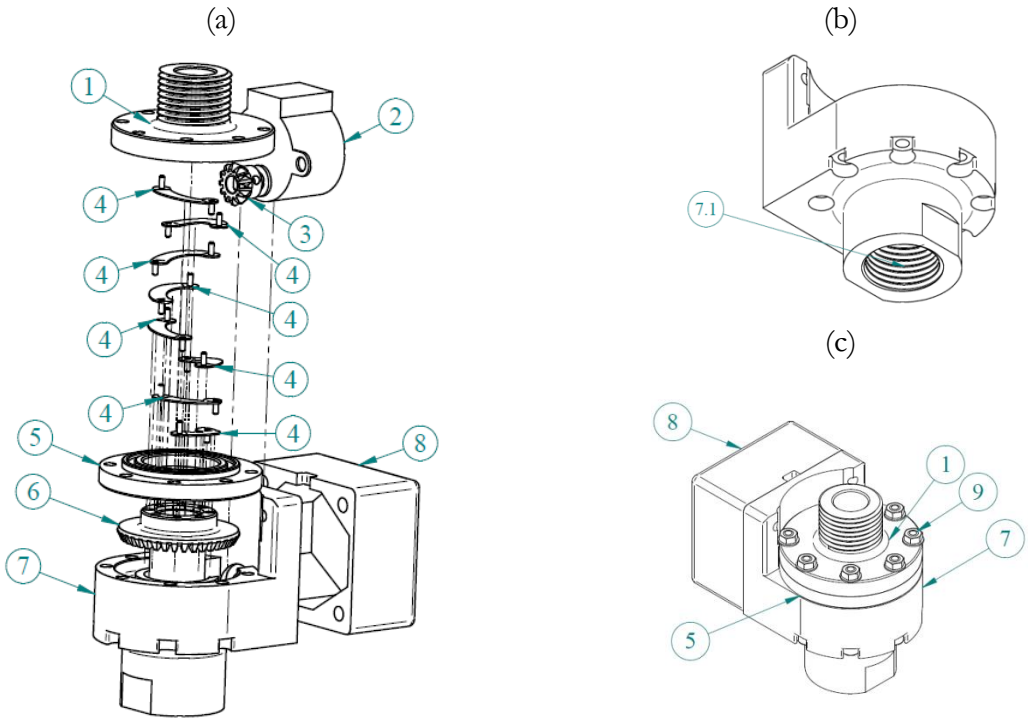

Figure 3.1. Detailed view of the improved prototype (a), new structure component (b) and assembly (c): blade holder (1), micro-stepper motor (2), motion/driving gear (3), blades (4), central body (5), driving gear (6), structure (7), micro-stepper motor protection (8), screws (9) and sealing rings (10).

The sprinkler prototype enables adjusting the orifice diameter from 4.9 to 12 mm, by using a micro-stepper motor electronically controlled. Increments in the micro-stepper motor angle (β), within the range 0° to 180°, decrease the orifice diameter according to a quadratic function ($D = -0.00012\beta^2 - 0.02084\beta + 11.33558$, R^2=0.996). Lower orifice sizes are mechanically possible but would require a stepper motor of higher torque than the one used during the experiments. Since the micro-stepper motor is electronically controlled, the orifice diameter may assume any value within the mentioned range and also may be remoted adjusted to comply with water requirements at the location being irrigated. The sprinkler may be used both in centre pivots and linear move systems.

3.2.2. Conventional sprinkler parameters

FSPSs and RSPSs, both from Senninger Inc. (Grand Island, NE, USA), were attached to the prototype and each was equipped with two different deflector plates (resulting in four combinations). The parameters of the sprinklers and their corresponding deflector plates are provided in Table 3.1.

Table 3.1. Manufacturer's specifications of the evaluated sprinklers and deflector plates.

Sprinkler		Type	Deflector plate		Number of grooves
	Super Spray	Fixed		Flat, no grooves	0
				Concave, thick grooves	48
	i-Wob	Rotating		Standard angle, small droplet	6
				Standard angle, medium droplet	9

Based on the equation proposed by Sobenko et al. (2018) for predicting the flow through orifices using the variable rate mechanism (Equation 3.1), two orifice sections with diameters of 4.93 mm (step angle 180°) and 6.94 mm (step angle 126°) were used. The discharge for each configuration was 0.62 and 1.20 $m^3\ h^{-1}$ for step angles of 180° and 126°, respectively, while operating the prototype under 103 kPa (15 psi). These sections of the orifice were selected to verify the water distribution patterns of the sprinkler operating at relatively high and low discharges. Higher values of discharge were not evaluated due to space constraints in terms of carrying out full-grid experiments indoors.

$$q = C_d\,\pi\left\{[X_3'\sin(\alpha_2')] + \left[\sqrt{r^2 - (r\cos(\alpha_1) - Z_2')^2} - r_1\right] - B'\right\}^2\sqrt{2gH} \qquad (3.1)$$

3.2.3. Experimental setup and water distribution measurement procedure

A structure simulating a centre pivot pendulum was mounted in the middle of the experimental plot (Figure 3.2). The prototype was coupled to a rigid pendulum at a height of 0.91 m from the ground, which corresponds to the height described by the sprinkler manufacturer (Senninger, 2018). At the inlet of the prototype, a pressure transmitter was connected to monitor the testing pressure, which was set at 103 kPa (15 psi). This operating pressure is commonly found for pressure regulators from several manufacturers (Fabrimar, 2018; Nelson, 2018;

Senninger, 2018) and it is used more frequently along a centre pivot lateral line (Frizzone et al., 2018). In addition, the other equipment required for pumping and pressure regulation can be seen in Figure 3.2.

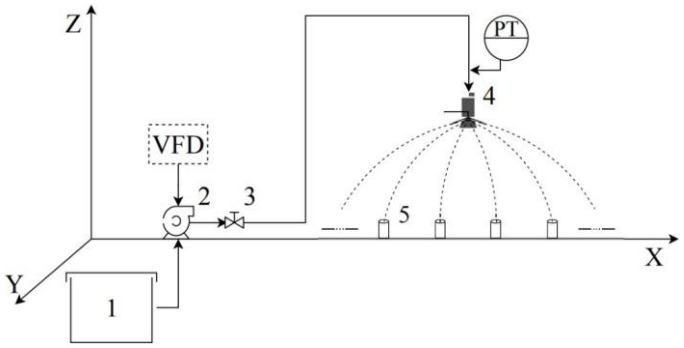

Figure 3.2. Instrumentation diagram of the indoor test apparatus: tank (1), pump (2), variable frequency driver (VFD), pressure-regulating valve (3), pressure transmitter (PT), sprinkler (4) and collectors (5).

The water distribution patterns were measured with a series of collectors (Fabrimar Inc., São Paulo, Brazil), arranged in full-grid collector arrays according to the requirements presented by ISO 8026 (International Organization for Standardization, 2009). All collectors used in the tests had a height of 80 mm and an opening diameter of 80 mm, which resulted in a collection area of 5.027 x 10^{-3} m^2. The spacing between the collectors was 0.5 x 0.5 m, arranged in 25 columns x 25 rows (Figure 3.3a). The values of the eight radii highlighted in Figure 3.3 were used to compute the mean radial profile of application. The sprinkler under test was positioned on the middle of the grid, as illustrated in Figure 3.3.

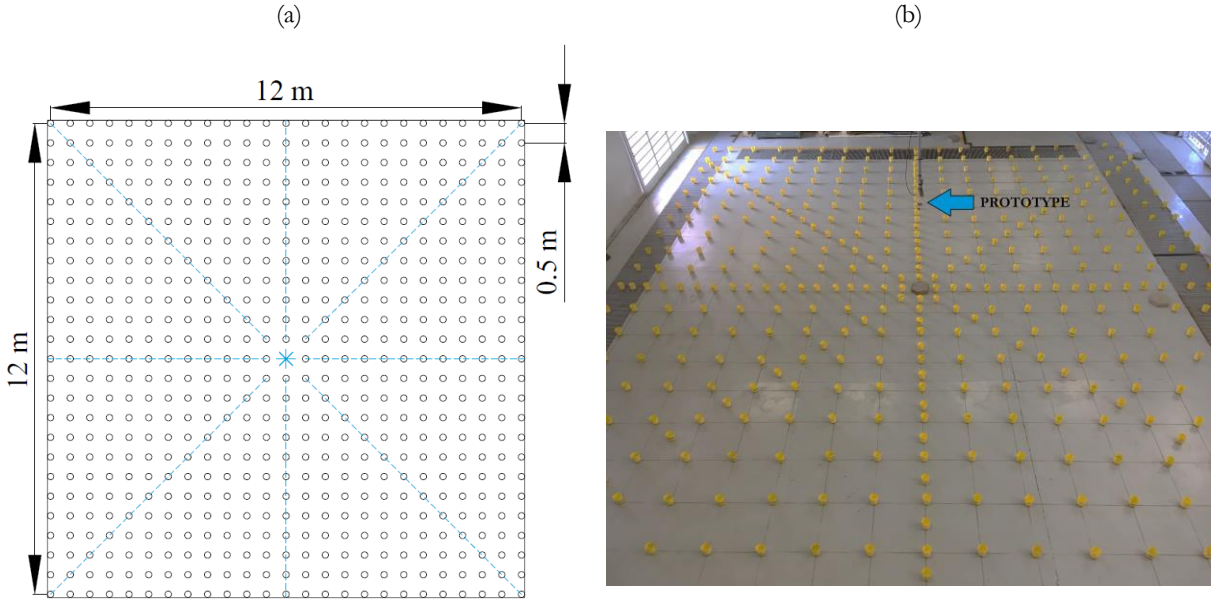

Figure 3.3. Collector arrangement for measurements of water distribution.

The test duration of each experiment was 1 h or less, depending on the application rate and water volume collected by the catch cans. Volumes were measured using graduated cylinders and then converted into water application rates using Equation (3.2). Since the sprinkler flow rate was higher than 0.075 $m^3\ h^{-1}$, the effective precipitation rate was assumed to be 0.26 mm h^{-1}, as recommended by ISO 8026 (International Organization for Standardization, 2009). Moreover, Table 3.2 provides detailed information for each test performed.

$$h = V\, S_C^{-1}\, t^{-1} \tag{3.2}$$

where:

h - precipitation rate (mm h^{-1});

V - volume collected in each collector (dm^3);

S_C - opening section of the collector (m^2); and

t - test duration (h).

Table 3.2. Summary of tests performed with the variable rate prototype.

Type	Deflector plate	Orifice diameter (step angle)	Test duration (h)	Flow rate ($m^3\ h^{-1}$)	Operating pressure (kPa)	Installation height (m)
FSPS	Flat	4.93 mm (180°)	0.417	0.62	103	0.91
		6.94 mm (126°)	0.333	1.20	103	0.91
	Concave	4.93 mm (180°)	0.450	0.62	103	0.91
		6.94 mm (126°)	0.333	1.20	103	0.91
RSPS	Small droplet	4.93 mm (180°)	1.000	0.62	103	0.91
		6.94 mm (126°)	0.833	1.20	103	0.91
	Medium droplet	4.93 mm (180°)	0.867	0.62	103	0.91
		6.94 mm (126°)	0.833	1.20	103	0.91

3.2.4. Overlap of sprayers

The data obtained were analysed and interpolated using the Surfer software (Golden Software Inc., Golden, CO, USA). The gridding method used was kriging, with a spacing accuracy of 0.01 m, which resulted in new matrices of 100 columns x 100 rows.

The individual water distribution matrices obtained for the FSPS and RSPS evaluations were mathematically overlapped to simulate the water application pattern produced by a section of a centre pivot or a linear move sprinkler machine. The goal was to obtain a 10.5-m section of fully overlapped water application in the lateral line. Two common values for sprinkler spacing were defined to perform the overlap simulations: 2 m and 3 m. Installing sprinklers at a single fixed distance along a lateral line facilitates the manufacturing process and the assembling of centre pivots or linear move sprinkler machines in the field (Frizzone et al., 2018). The required

number of sprinklers varied depending on the spacing and the effective jet length of the sprayer attached to the prototype; 5 (for 3 m spacing) and 9 (for 2 m spacing) for FSPSs; 7 (for 3 m spacing) and 11 (for 2 m spacing) for RSPSs. Figure 3.4 shows an example of the procedure used to overlap the water application for RSPSs equipped with medium droplet plates and operating with 6.94-mm orifice diameters. (For further detail of the overlapping procedure, see Faci et al. [2001].)

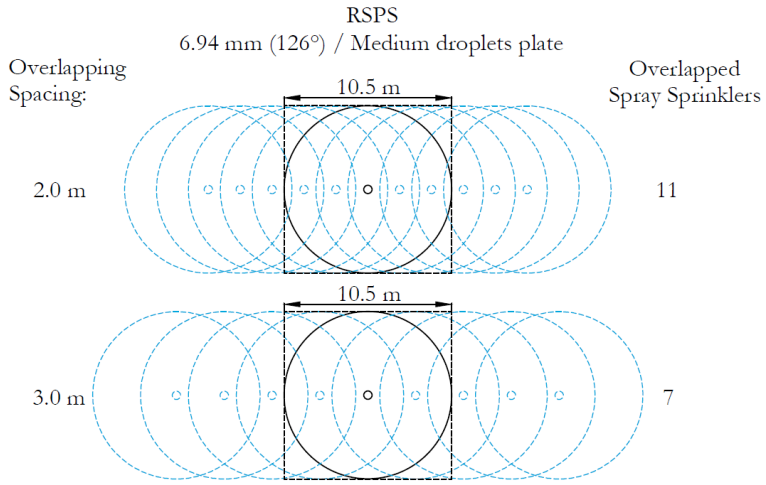

Figure 3.4. Schematic example of the mathematical procedure used for simulation of the overlapping of sprinkler spray patterns.

The Christiansen coefficient of uniformity (CUC) was calculated for the fully overlapped section of the lateral using Equation (3.3). The CUC simulates the uniformity of the lateral travel of irrigation over a parallel line of the full-grid collector arrays. Although this coefficient is adequate for analysing the data presented here, it is not suitable for the characterization of a complete centre pivot lateral due to the increase in the irrigated area produced by each sprinkler towards the end of the lateral line (Keller and Bliesner, 1990; Faci et al., 2001).

$$CUC = \left(1 - \frac{\sum_{i=1}^{n} |h_i - \bar{h}|}{n\,\bar{h}}\right) 100 \qquad (3.3)$$

where:

CUC - Christiansen coefficient of uniformity (%);

h_i - precipitation rate of the *i*-th observation (mm h^{-1});

$\bar{h}$ - average precipitation rate (mm h^{-1}); and

n - number of observations.

In addition, the precipitation rate curves of and irrigation zone irrigated by a set of variable rate sprinklers equipped with FSPSs and RSPSs were simulated and compared to the soil

infiltration rate curve to identify risk of surface runoff. For this, as in the procedure for determining the CUC, we use the fully overlapped section of the lateral obtained by simulating a lateral line of a centre pivot traveling over a parallel line of the full-grid collector arrays (Faci et al. 2001). Thus, the application rate was computed at each time interval given by the ratio between the new spacing between collectors and the displacement velocity of the last tower. Finally, as the water application profile did not present a symmetrical pattern, the trapezoidal numerical integration rule was used to calculate the applied accumulated depth after the lateral line passage over the irrigated zone. Moreover, just for demonstration purposes, the application rates were compared with the infiltration rate presented by Cunha et al. (2015) for the location of Rio Largo, Alagoas, Brazil. The soil in this location is a typical dystrophic cohesive yellow Latosol, characterized by a sandy loam texture and a bulk density of 1280 kg m^{-3} and cultivated under a minimum tillage system.

3.3. Results and discussion

3.3.1. The improved prototype

Figure 3.5a shows all components of the new prototype developed, and Figure 3.5b shows the assembled prototype.

Figure 3.5. Images of the new prototype.

3.3.2. Water distribution patterns of individual sprinklers

Figure 3.6 represents the wetted patterns generated by the FSPSs (Figure 3.6a–d) and RSPSs (Figure 3.6e–h) attached to the prototype. The wetted patterns presented similar profiles despite differences in the magnitude of application rates. FSPSs applied water at a higher rate

closer to the sprinkler and RSPSs distributed water more evenly, at a lower application rate and further from the sprinkler (Figure 3.6).

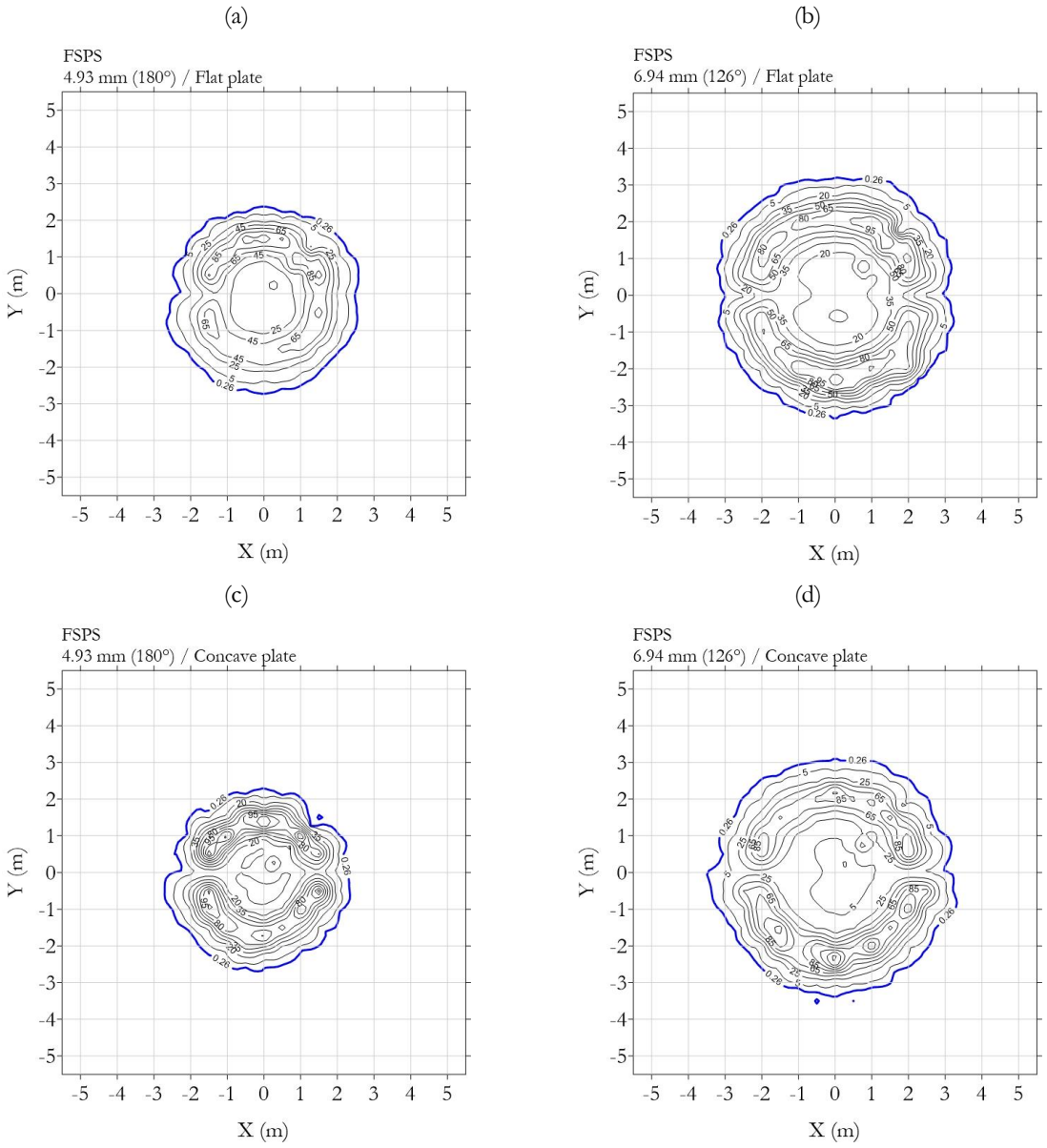

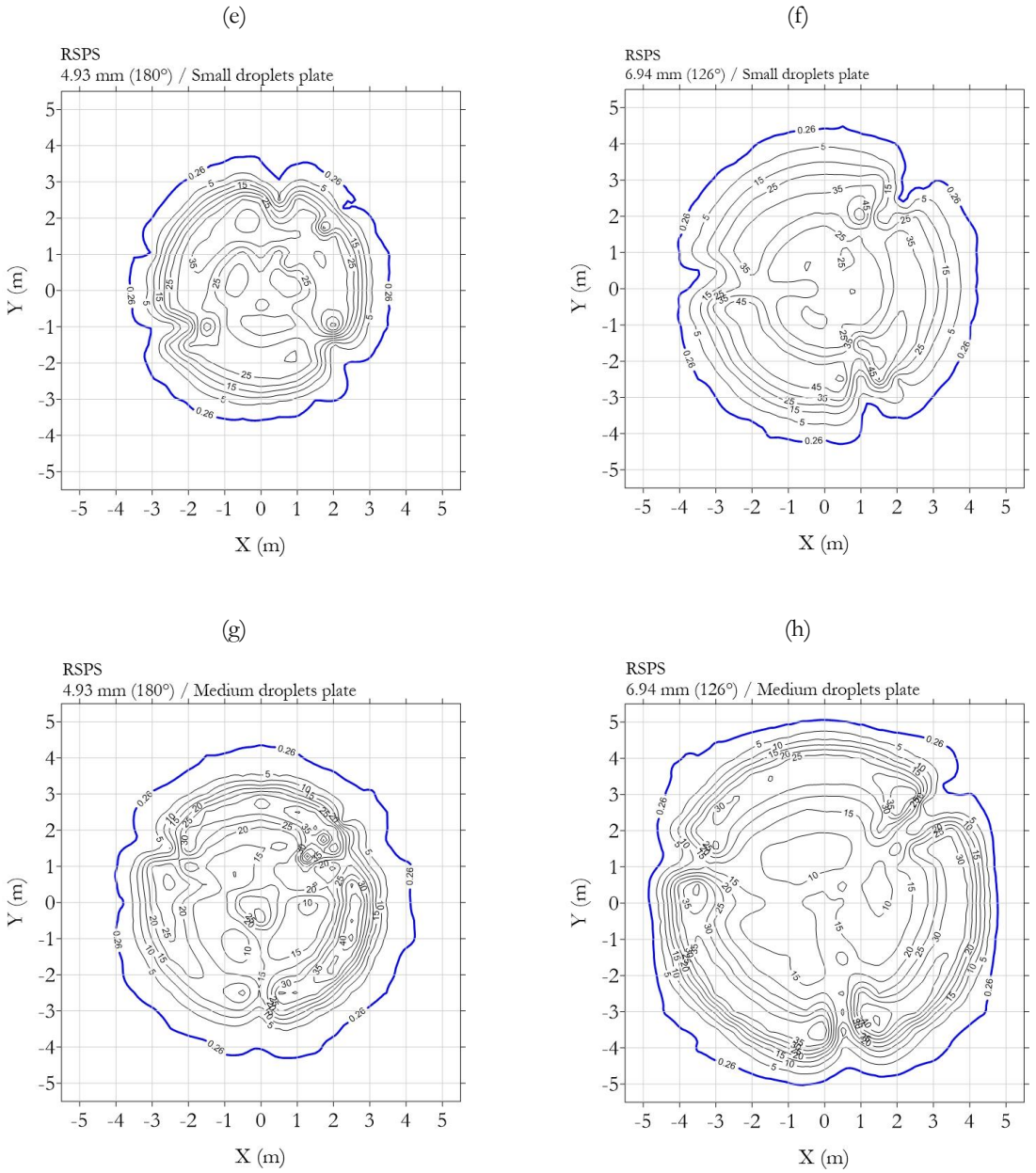

Figure 3.6. Wetted patterns (mm h^{-1}) of the prototype operating with two orifice sizes and four different deflector plates.

The FSPSs tended to distribute most of the water over both sides of the sprinkling axis, while the area around the sprinkling axis received less water, similar to a wetted circular "crown", because the deflector plate reduced the velocity of the water and the initial trajectory velocity across the plate was less than the jet velocity (Kincaid, 1996). For RSPSs, the application rates declined gradually with increasing distance from the axes. With an increase in orifice diameter, the coverage width of RSPSs increased, the precipitation rates also increased and the peak of the application rate was further from the sprinkler.

Figure 3.7 shows the mean application rate distribution profiles for FSPSs and RSPSs: for the same conventional sprinkler types, the profiles are similar, despite differences in

magnitude. By enlarging the orifice section, the location of the higher application rate shifted from around 1.7 m to 2.2 m and from 1.5 m to 2.1 m away from the sprinkler for flat and concave deflector plates, respectively (Figure 3.7a–b). With an increase in orifice section, the application rate shifted from 1.8 m to 2.5 m and from 2.7m to 3.8 m for the small and medium droplet plates, respectively (Figure 3.7c–d).

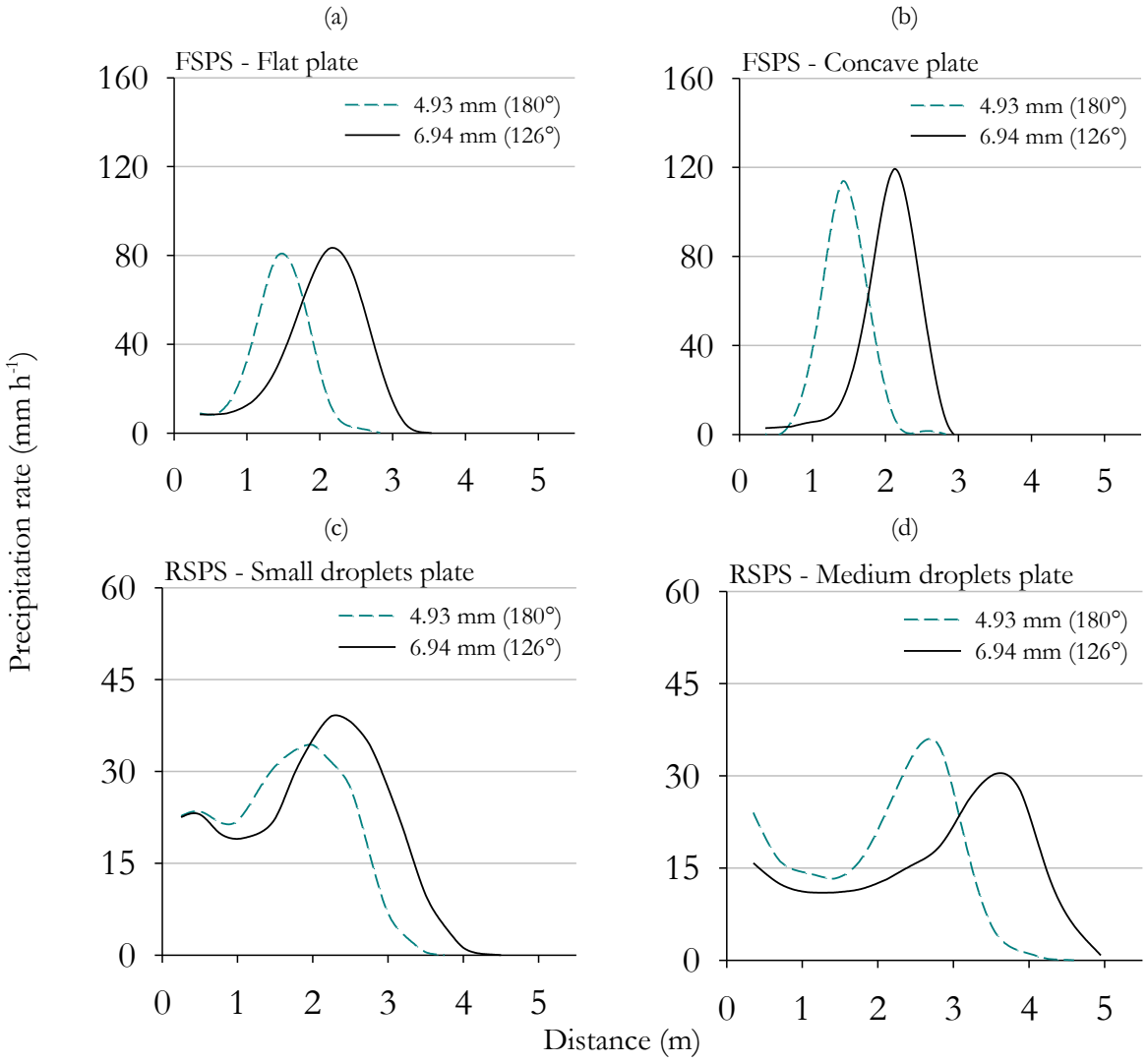

Figure 3.7. Mean radial precipitation profiles of the prototype operating with two orifice sizes and four different deflector plates.

For the same sprinkler, the effective wetted radius and wetted area increased as the discharge section increased, i.e. with the reduction of the step angle. The wetted radius increased by an average of 25.4% and 18.6% for FSPSs and RSPSs, respectively. The effective wetted area increased by an average of 67.8% for FSPSs and 42.4% for RSPSs (Table 3.3).

Table 3.3. Observed wetted radii and areas of the prototype operating with two orifice sizes and four different deflector plates.

Type	Deflector plate	Orifice diameter (step angle)			
		4.93 mm (180°)	6.94 mm (126°)	4.93 mm (180°)	6.94 mm (126°)
		Wetted radius (m)		Wetted area (m^2)	
FSPS	Flat	2.7	3.3	20.6	33.2
	Concave	2.7	3.5	18.5	32.7
RSPS	Small droplet	3.6	4.2	40.7	56.0
	Medium droplet	4.2	5.1	54.9	80.8

The FSPSs showed peaks of water application clearly visible near the borders of the wetted area, corroborating the results obtained by Faci et al. (2001) and Jiao et al. (2017) when evaluating FSPSs in outdoor conditions and by Sayyadi et al. (2014) when evaluating the same deflector plates indoors. In contrast, the RSPSs presented two peaks of water application, one near to the sprinkler outlet and the other at up to 75% of the effective wetted radius. These RSPS distribution profiles were different from those obtained by Faci et al. (2001), Sourell et al. (2003), Playán et al. (2004) and Jiao et al. (2017) when evaluating RSPSs from another manufacturer and at different installation heights.

These differing water distributions between FSPSs and RSPSs were attributable primarily to the different structure of the deflector plates presented in Table 3.1. The black flat deflector plate used for the FSPS has no grooves, while the blue concave deflector plate has 48 grooves with unique shapes, angles and depths. However, the deflector plate used for RSPS has grooves with a combination of multiple shapes and depths, including the feature of rotability, which could generate multiple streams and enable improvement in the water distribution in the presence of diverse soil, plant and climate conditions.

With regard to existing technologies for applying water at variable rates by changing the discharge section, the prototypes developed by King and Kincaid (2004) and Armindo et al. (2010) both tested RSPSs equipped with four- and six-groove deflector plates. When the prototype developed by King and Kincaid (2004) was tested under similar operating conditions to those used in this work, i.e. at a pressure of 138 kPa and an orifice diameter of 4.56 mm, it also resulted in two peaks of water application in its profile, one at approximately 4 m and one of greater intensity near the border of the wetted radius. However, in all tests carried out by Armindo and Botrel (2012), the prototype presented a single peak of water application that was well defined at 4 m and 5 m for the four and six-groove deflector plates, respectively.

3.3.3. Uniformity of overlapped water distribution

The uniformity of water application for a lateral line with sprinkler spaced at 2 or 3 m intervals was simulated for all of the individual evaluations (Table 3.4).

Table 3.4. Christiansen coefficient of uniformity (CUC) for the variable rate prototype operating with two orifice sizes, four deflector plates and two sprinkler spacings.

Type	Deflector plate	Orifice diameter (step angle)			
		4.93 mm (180°)	6.94 mm (126°)	4.93 mm (180°)	6.94 mm (126°)
		Spacing 2 m		Spacing 3 m	
FSPS	Flat	82.5%	82.2%	65.3%	68.0%
	Concave	72.1%	85.7%	61.2%	66.7%
RSPS	Small droplet	93.6%	97.7%	88.5%	95.4%
	Medium droplet	95.9%	98.6%	94.3%	87.2%

The CUC values obtained indicate that the RSPSs presented better water distribution than the FSPSs in all the studied conditions. As the spacing between the sprinklers increased, the CUC values of all sprinklers decreased, especially for black flat and blue concave deflector plates. The CUC of RSPSs with small droplet deflector plates was less sensitive to an increase in sprinkler spacing, decreasing by only 5.4% and 2.3% for the 4.93-mm and 6.94-mm orifice diameters, respectively. For the 4.93-mm orifice diameter, on average, the FSPSs and RSPSs decreased by 17.9% and 3.5%, respectively. For the 6.94-mm orifice diameter, when the effective wetted area increased, the CUC values were not particularly sensitive to the increase in the sprinkler spacing, decreasing on average by 19.7% and 6.7% for FSPSs and RSPSs, respectively (Table 3.4).

Jiao et al. (2017) also observed reductions in CUC values with an increase in sprinkler spacing; moreover, with an increase in the discharge section, CUC values tended to decrease slowly relative to increases in sprinkler spacing for FSPSs and RSPSs. Playán et al. (2004) obtained superior CUC values for two RSPSs evaluated in relation to FSPSs, employing the same overlap spacing but increasing the discharge sections and generating an average CUC increase of 22%.

To achieve a uniform water distribution pattern, Frizzone et al. (2018) recommended that the sprinklers should be spaced closely to enable adequate overlap. For FSPSs, this means that the sprinklers must be closer; therefore, a larger number of sprinklers are required, which will result in a higher application rate. Moreover, the wetted circular "crown" phenomenon previously mentioned for FSPSs became more clearly visible with an increase in orifice diameter and sprinkler spacing. When the sprinkler spacing increased, the continuity of water distribution along the axis of the sprinkler appeared to decrease, presenting as a continuous circular water

distribution along the axes, with lower precipitation rates in the middle of the circle and higher precipitation rates at the borders of the circle (Figure 3.8).

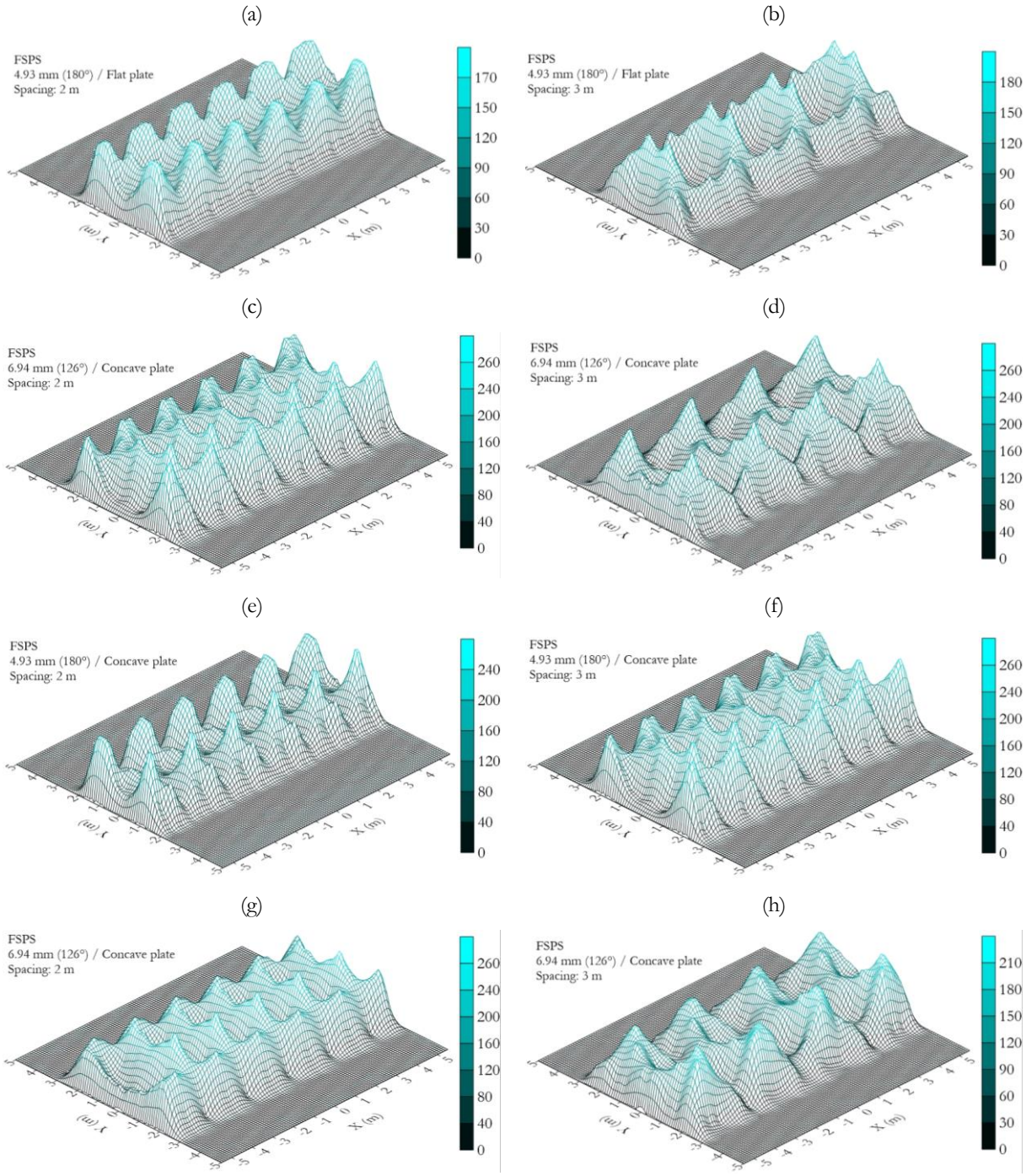

Figure 3.8. Water distribution characteristics in irrigation lateral equipped with FSPSs with the variable rate prorotype operating with different orifice diameters, motor step angles, deflector plates and sprinkler spacing.

For RSPSs, when the sprinkler spacing was increased to 3 m, the continuity of water distribution along the axis of the sprinkler appeared to decrease more smoothly than for FSPSs and the regions of higher and lower precipitation rates alternated along the sprinkling axis (Figure 3.9). Moreover, based on the CUC values, the phenomenon of jet inversion mentioned by

Sobenko et al. (2018) did not appear to impair water distribution uniformity, especially when the prototype was coupled to RSPSs (Figure 3.9).

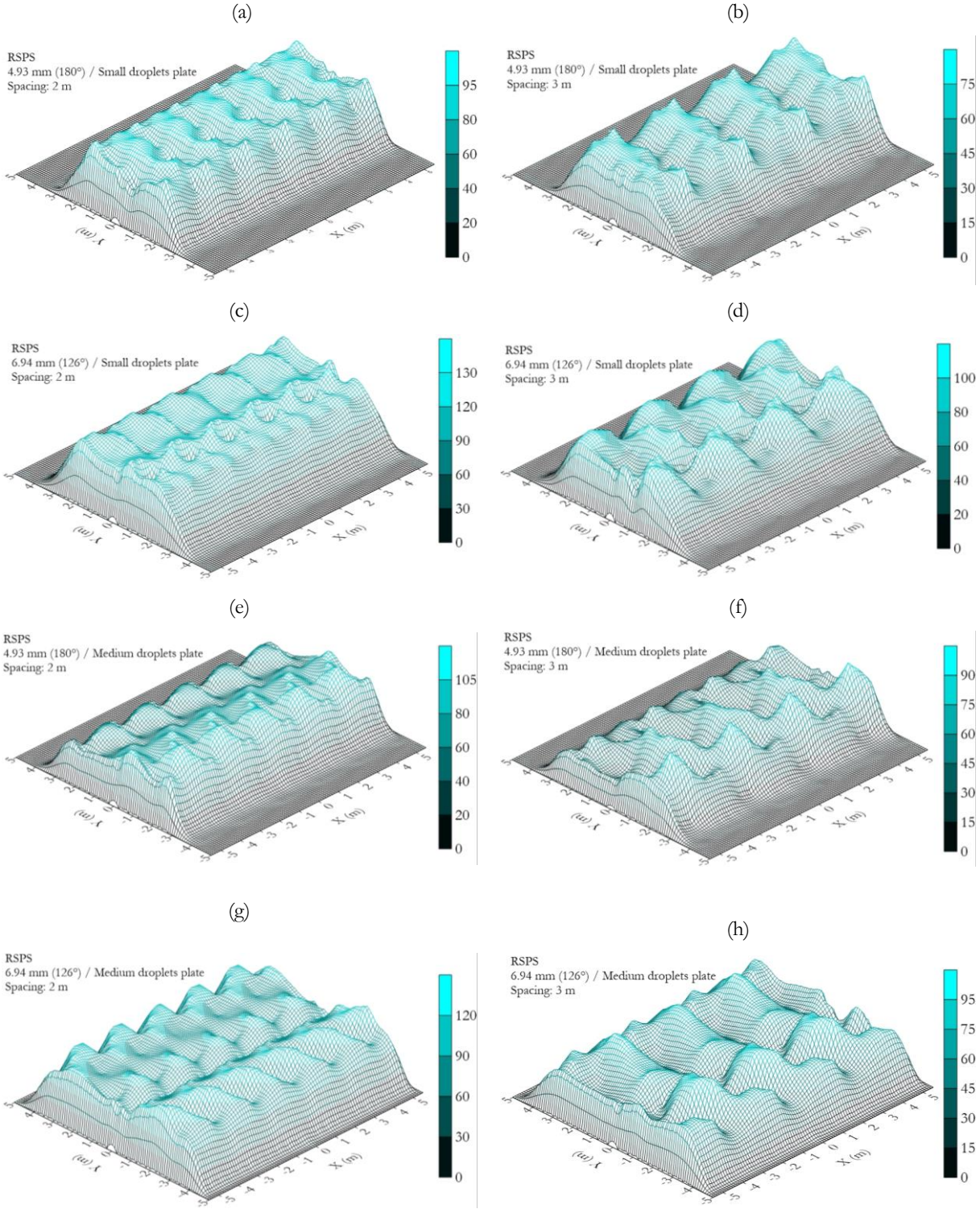

Figure 3.9. Water distribution characteristics in irrigation lateral equipped with RSPSs with the variable rate prorotype operating with different orifice diameters, motor step angles, deflector plates and sprinkler spacing.

Figure 3.10 presents an application of the simulated patterns of the precipitation rate versus time for an irrigation lateral line sprinkler equipped with the prototype developed. For this

application, we supposed a centre pivot equipped with variable rate technology irrigatin an area of 81.7 ha and operating at a speed equal to 128.7 m h^{-1} at the last tower, with a time of revolution of 23 h. For comparison purposes, the applied water depth during the wetting time was calculated and an irrigation soil infiltration curve was plotted, considering an irrigation zone in the last tower in which a set of sprinklers may have their orifice diameters adjusted to comply with water requirements at the irrigated zone.

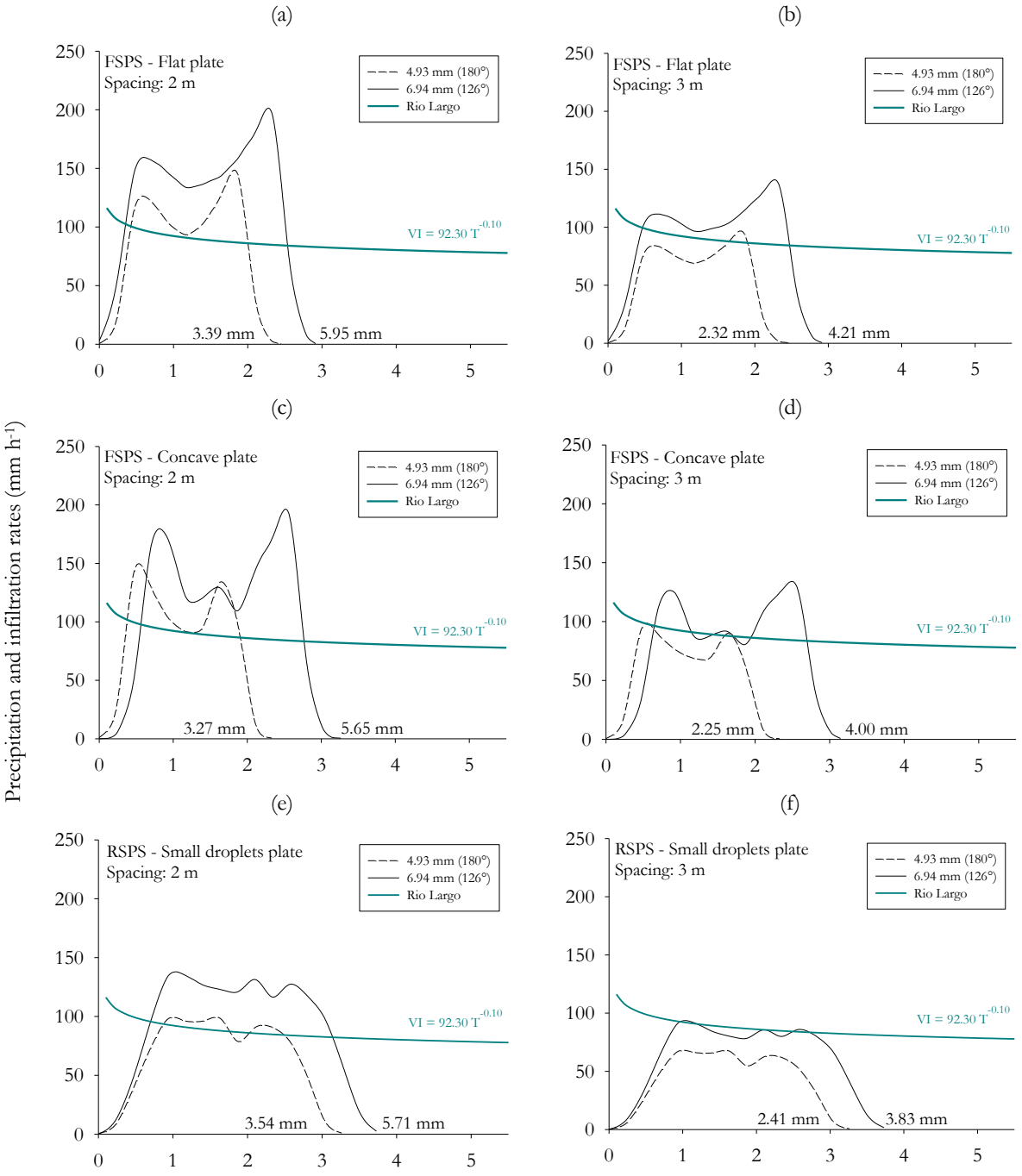

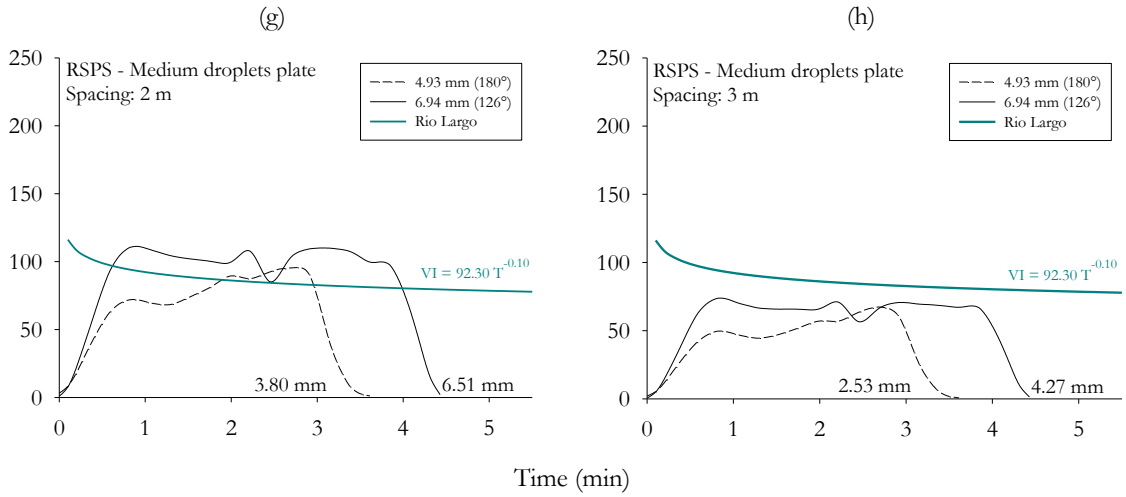

Figure 3.10. Precipitation rate versus irrigation time in irrigation lateral equipped with FSPSs and RSPSs with the variable rate prototype operating with different orifice diameters, motor step angles, deflector plates and sprinkler spacing. Application curves are compared to the soil infiltration rate of Rio Largo, Alagoas, Brazil.

The FSPSs present higher precipitation rates compared to RSPSs with the same nozzle diameters and sprinkler spacing, which could increase the potential for surface runoff and soil erosion (King and Bjorneberg, 2011). When the application rate curve exceeds the infiltration velocity curve, surface runoff will occur; this can be quantified as the difference between the irrigation application and the infiltration curve (DeBoer and Chu, 2001; Frizzone et al., 2018). Therefore, under the conditions reported here, a high potential for surface runoff for FSPSs with smaller orifice diameter and spacing can be observed in Figure 3.10a and 3.10c. Figure 3.10e–h also indicate the adequacy of the prototype when attached to RSPSs, mainly for larger sprinkler spacings, due to its capability in preventing runoff water losses and other aforementioned characteristics.

3.4. Conclusions

The water distribution patterns of the prototype coupled to FSPSs and RSPSs were determined through a set of indoor experiments. Comparing similar testing conditions for both groups of sprinklers, higher values of CUC, larger wetted areas and lower application rates and surface runoff potentials were observed for RSPSs. Moreover, RSPSs were less sensitive to increased sprinkler spacing. According to the simulated CUC values, the phenomenon of jet inversion found in an earlier study (Sobenko et al., 2018) apparently did not impair water distribution uniformity, especially when the prototype was coupled to RSPSs, which had sprinkling uniformities of up to 98.6%. In terms of water distribution characteristics, the prototype coupled to FSPSs and RSPSs is suitable for variable rate sprinkler irrigation.

References

Armindo, R. A., and Botrel, T. A. (2012). Performance and radial distribution profiles of a variable flow rate sprinkler developed for precision irrigation. **Scientia Agricola**, 69(2), 160–167.

Armindo, R. A., Botrel, T. A., and Garzella, T. G. (2010). Flow rate sprinkler development for site-specific irrigation. **Irrigation Science**, 29, 233–240.

Cunha, J. L. X. L., Coelho, M. E. H., Albuquerque, A. W., Silva, C. A., Silva Júnior, A. B., and Carvalho, I. D. E. (2015). Water infiltration curve rate in yellow Latosol under different soil management systems. **Revista Brasileira de Engenharia Agrícola e Ambiental**, 19(11), 1021–1027.

DeBoer, D. W. (2002). Drop and energy characteristics of a rotating spray-plate sprinkler. **Journal of Irrigation and Drainage Engineering**, 128(3), 137–146.

DeBoer, D. W., and Chu, S. T. (2001). Sprinkler technologies, soil infiltration and runoff. **Journal of Irrigation and Drainage Engineering**, 127(4), 234–239.

Dong, X., Vuran, M. C., and Irmak, S. (2013). Autonomous precision agriculture through integration of wireless underground sensor networks with center pivot irrigation systems. **Ad Hoc Networks**, 11, 1975–1987.

Dukes, M. D., and Perry, C. (2006). Uniformity testing of variable-rate center pivot irrigation control systems. **Precision Agriculture**, 7, 205–212.

Esses, J. S., Berman, P., Bloom, A. I., and Sosna, J. (2011). Clinical application of physical 3D models derived from MDCT data and created by rapid prototyping. **American Journal of Roentgenology**, 196, 683–688.

Evans, R. G., LaRue, J., Stone, K. C., and King, B. A. (2012). Adoption of site-specific variable rate sprinkler irrigation systems. **Irrigation Science**, 31, 871–887.

Fabrimar. (2018). **Performance table**. Retrieved from http://www.fabrimar.com.br/categoria?irrigacao=produtos-para-pivo-central

Faci, J. M., Salvador, R., Playán, E., and Sourell, H. (2001). Comparison of fixed and rotating spray plate sprinklers. **Journal of Irrigation and Drainage Engineering**, 127(4), 224–233.

Frizzone, J. A., Rezende, R., Camargo, A. P., and Colombo, A. (2018). **Irrigação por aspersão: sistema pivô central**. Maringá: Eduem.

International Organization for Standardization. (2009). **Agricultural irrigation equipment – Sprayers – General requirements and test methods**. (ISO/DIS Standard No. 8026). Retrieved from https://www.iso.org/obp/ui/#iso:std:iso:8026:ed-3:v1:en.

Jiao, J., Wang, Y., Han, L., and Su, D. (2017). Comparison of water distribution characteristics for two kinds of sprinklers used for center pivot irrigation systems. **Applied Sciences**, 421(7).

Keller, J., and Bliesner, R. D. (1990). **Sprinkle and trickle irrigation**. New York, NY: Van Nostrand Reinhold.

Kincaid, D. C. (1996). Spraydrop kinetic energy from irrigation sprinklers. **Transactions of the ASAE**, 39(3), 847–853.

King, B. A., and Bjorneberg, D. L. (2011). Evaluation of potential runoff and erosion of four center pivot irrigation sprinklers. **Applied Engineering in Agriculture**, 27(1), 75–85.

King, B. A., and Kincaid, D. C. (2004). A variable flow rate sprinkler for site-specific irrigation management. **Applied Engineering in Agriculture**, 20(6), 765–770.

Kranz, W. L., Evans, R. G., Lamm, F. R., O'Shaughnessy, S. A., and Peters, R. T. (2012). A review of mechanical move sprinkler irrigation control and automation technologies. **Applied Engineering in Agriculture**, 28(3), 389–397.

Nelson. (2018). **Irrigation technology for the future – 2018 product catalog**. Retrieved from http://nelsonirrigation.com/media/general/2018_CATALOG_NO_LR.pdf

Ouazaa, S., Burguete, J., Paniagua, M. P., Salvador, R., and Zapata, N. (2014). Simulating water distribution patterns for fixed spray plate sprinkler using the ballistic theory. **Spanish Journal of Agricultural Research**, 12(3), 850–863.

Playán, E., Garrido, S., Faci, J. M., and Galán, A. (2004). Characterizing pivot sprinklers using an experimental irrigation machine. **Agricultural Water Management**, 70, 177–193.

Sayyadi, H., Nazemi, A. H., Sadraddini, A. A., and Delirhasannia, R. (2014). Characterising droplets and precipitation profiles of a fixed spray-plate sprinkler. **Biosystems Engineering**, 119, 13-24.

Senninger. (2018). **Mechanized irrigation: low pressure-high performance**. Retrieved from https://www.senninger.com/sites/senninger.hunterindustries.com/files/senninger-pivot-irrigationproducts-catalog.pdf

Sobenko, L. R., Camargo, A. P., Botrel, T. A., Santos, J. D. M., Frizzone, J. A., Oliveira, M. F., and Silva, J. V. L. (2018). An iris mechanism for variable rate sprinkler irrigation. **Biosystems Engineering**, 175, 115–123.

Sourell, H., Faci, J. M., and Playán, E. (2003). Performance of rotating spray plate sprinklers in indoor experiments. **Journal of Irrigation and Drainage Engineering**, 129(5), 376–380.

Stone, K. C., Sadler, E. J., Millen, J. A., Evans, D. E., and Camp, C. R. (2006). Water flow rates from a site-specific irrigation system. **Applied Engineering in Agriculture**, 22(1), 73–78.